Chapter 2

Design, synthesis and birefringent properties of hydrogels derived from complex metallogelator containing copper(II), 2,2'-bipyridine and myo-inositol

Chapter 2 Design, synthesis and birefringent properties of hydrogels derived from complex metallogelator containing copper(II), 2,2'-bipyridine and myo-inositol

2.1 Introduction

The metallogels[1] as described in the previous chapter 1 have unique properties owing to the presence of metal ions/atoms in the supramolecular structure of the gel. The supramolecular gelator systems are formed because of the non-covalent[2–8] interactions like H-bonding and π-π stacking.[9–11] The metallogels are characterized by measuring T_{gel} by inverted vial method. The morphological properties[12–14] of the gels indicate the presence of fibrous structures which immobilize the solvent. The presence of the fibrous structures is characterized by SEM and TEM analysis. Most of the supramolecular gels reported so far have entangled fibers responsible for gel formation as seen in various microscopic images. However, as far as birefringence in gels is concerned, such reports are scanty.

Amongst the very few reports of gels showing birefringent behaviour, amide-derived organogels having π-conjugated phenylethyl frameworks have been reported to exhibit columnar and smectic liquid crystalline phases on heating.[15]

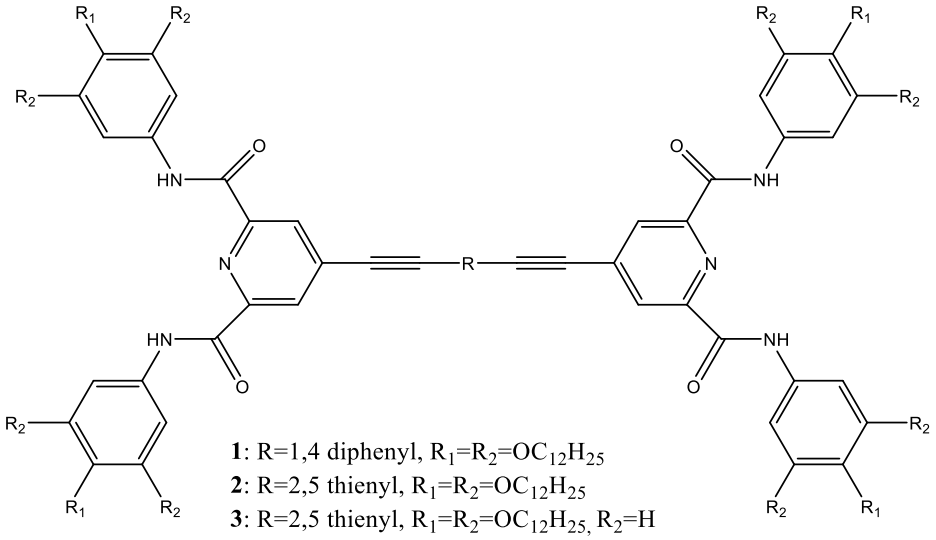

Figure 2.1.1 Figure showing the organogelator molecules featuring Phenylethynyl framework with Elaborated Long-Chain Pyridine-2,6-Dicarboxamides (Reported by Shih-Sheng Sun *et al*) [25].

The compounds 1,2,3 and 4 as shown in fig. 2.1.1 give organogels that exhibit viscous liquid crystal like properties.

Another of such reports included a dipeptide based L-pro-L-val organocatalytic gels[16] which showed the presence of spherulites.[17,18] Spherulites are birefringent structures with radial symmetry in 3-dimensions and a possess a circular symmetry in a thin section when observed under Polarized Optical Microscopy (POM).

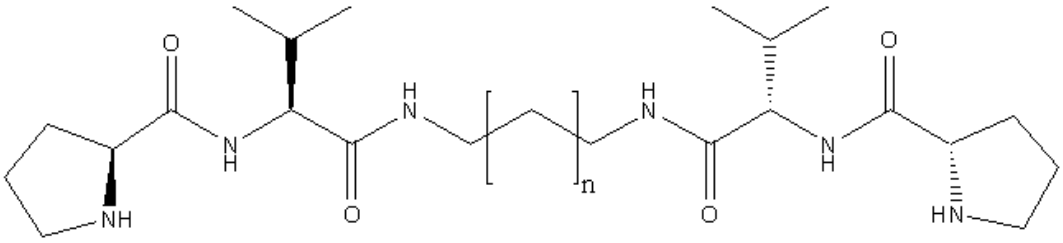

5 a-c (n=1,4,6)

Figure 2.1.2 Dipeptide based L-Pro-L-Val which exhibit spherulite structures under POM (Reported by Juan F. Miravet *et al*).[16]

Compounds 5 a-c (fig. 2.1.2) being peptides are expected to show an aggregation pattern similar to β-sheets. In order to get more insight in the aggregation pattern the authors performed the POM of the above organogels which exhibited the spherulite kind of formation.

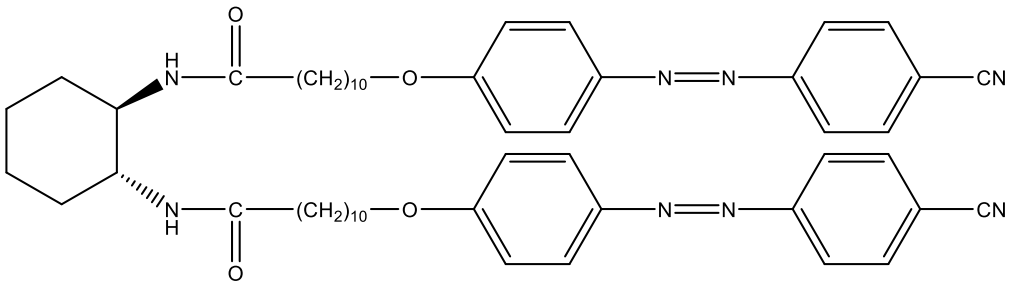

Figure 2.1.3 Figures showing the structure of photoresponsive gelator (reported by Kato *et al*).[19]

Kato et al reported photoresponsive gels formed by the photoresponsive gelator moiety shown in **Figure 2.1.3**. The photoresponsive LC gels were reported for the mixtures of nematic liquid crystal and a hydrogen-bonded chiral gelator having photochromic azobenzene moieties **(Figure 2.1.3)**. Since the composite gels contain LC phase as well as photoresponsive gelator molecules the gels are thermo- as well as photo-sensitive.[19–21]

Composite liquid crystalline physical gel of photochromic azobenzene moieties as hydrogen bonded chiral gelators and typical rod-like LC molecules like 4-butyl-4'-cyanophenyl exhibited phase transformations on exposure to UV light or at elevated temperatures.[19,20,22,23]

Arun K. Nandi et al reported a silver(I) coordination complex of melamine which resulted in the formation of metastable hydrogel at 1:1 ratio, however a stable gel was obtained at 1:2 molar ratio of Ag(I): Melamine. The hydrogels are very sensitive to anion and pH change and were reported to show excellent dye absorbing properties.

They reported the formation of gel as a bicomponent supramolecular gel stating that even though melamine is known to provide a good coordination environment to the metal ions, they did not find any proof for the formation of a metallogel. In the same work the authors report that Ag(I) coordinates with melamine molecules through the nitrogen atoms of its triazine ring. The POM analysis of the gels formed at 1:1 and 1:2 ratios show birefringent nature of the gel fibres indicating the presence of anisotropy in the structure of the hydrogels.[24]

Tanmaya Pathak *et. al.* have reported the formation of a nickel-based nano metallogel. The gels are reported to be formed using $NiCl_2.6H_2O$, in the presence of a wide range of amines, cis-$Ni(OMe)_2(MeOH)_4$ as one of the major components of the gel. The POM images of these gels revealed the presence of elongated fibres which are responsible for the formation of gel network, the authors, however, did not observe birefringent property in these gels.[25]

Though scarce, the literature reports clearly indicate that the gels can possess birefringent properties. There have been few examples where these properties were explored or reported in organogels, however, the reports of birefringent behaviour in metallogels are even more rare. These kinds of birefringent properties are observed owing to the anisotropy or dissymmetry present in the supramolecular assembly or the gelator molecules forming the gel network. This property in usually observed when the gel is converted to a xerogel. Birefringent properties if obtained by the presence of a liquid crystalline moieties in the framework of the gel, it can make the gel thermo-sensitive.[26] Few gels show birefringent properties after the loss of solvent mobilized by them, the loss of solvent introduces anisotropy leading to the birefringent behavior of the gels. This type of birefringent property is similar to lyotropic liquid crystals and can be explored to make the gels solvent sensitive.

The birefringent property if present in the gels, can be exploited for various purposes right from medicinal applications to non-linear optics.[27] The variation in birefringence with the differing water content, pH and other properties of normal and cancer cells can be used as a diagnostic tool. The birefringent properties of the gels can also be used in developing non-linear optical materials. These hydrogels have an advantage over liquid crystals in a way that it is more convenient to form a film of the gels compared to that of liquid crystals.

The work in this chapter includes the synthesis of a supramolecular metallo-hydrogel formed by a trinuclear copper(II) complex involving myo-inositol and 2,2'-bipyridine, that shows birefringent behaviour with quaternary assembly under polarized light. Unlike the earlier reports, no liquid crystalline material or chiral compound was added to form a composite with the gelator. Rather the property is inherited from the quaternary assembly of the complex molecules in the gel itself. This is for the first time that such detailed outlook of birefringent properties in metallogelator system has been explore and reported. Variation in various parameters and their effects on the morphological properties of the metallogels has been studied and discussed in this chapter.

The trinuclear complex cation[28] **$[Cu_3(H_3ins)(bipy)_3]^{3+}$** is expected to have specific stereochemistry due to the presence of myo-inositol and the organization of three $[Cu\text{-}bipy]^{2+}$ units, which may attribute interesting optical properties to the supramolecular assembly formed in the presence of various anions. In order to examine this possibility, microscopic studies of the gels were carried out. The interesting characteristics revealed in the microscopic studies have been discussed in this chapter.

2.2 Experimental section

2.2.1 Materials

Cupric acetate monohydrate and 2,2'-bipyridine (bipy) were purchased from Qualigens; myo-inositol (ins) was obtained from Sigma-Aldrich, NaOH was obtained from Merck and KOH was obtained from Qualigens. Cupric carbonate was procured from local manufacturers; formic acid and propionic acid were obtained from Merck. Cupric formate and cupric propionate were prepared by reacting formic acid and propionic acid with cupric carbonate, respectively. All the chemicals were used for synthesis without further purification. Triple distilled water was used as solvent for the synthesis of gels.

2.2.2 Synthesis

The reaction of inositol with 3 equivalents of copper and varying amounts of 2,2'-bipyridine (bipy) was carried out. No gel formation was observed with 1 or 2 equivalents of bipy at all pH values and varying concentrations. The reaction of 10 mL of a 2.5% aqueous solution (1.388 mmol) of myo-inositol was carried out with 3 equivalents of $[Cu(bipy)]^{2+}$ complex obtained by reacting 0.638 g (4.163 mmol) of cupric formate and 0.650 g (4.163 mmol) of bipy in 25 mL of water **(Scheme 2.2.2.1)**. Subsequently, the pH was raised to 12 with aqueous sodium hydroxide. The solution was held at 60–70 °C for 30 minutes and allowed to settle at room temperature to obtain the gel (111). Repeating the same procedure with cupric acetate (0.831 g, 4.163 mmol) and cupric propionate (0.8725 g, 4.163 mmol) resulted in the formation of green transparent gels, 112 and 113, respectively. The same procedure was repeated using equivalent amounts of all reagents but using aqueous potassium hydroxide as alkali in place of sodium hydroxide to get the gels 121, 122, and 123, respectively, with formate, acetate and propionate. The gelation was confirmed by the inverted test tube method **(Figure 2.3.1.1)**.

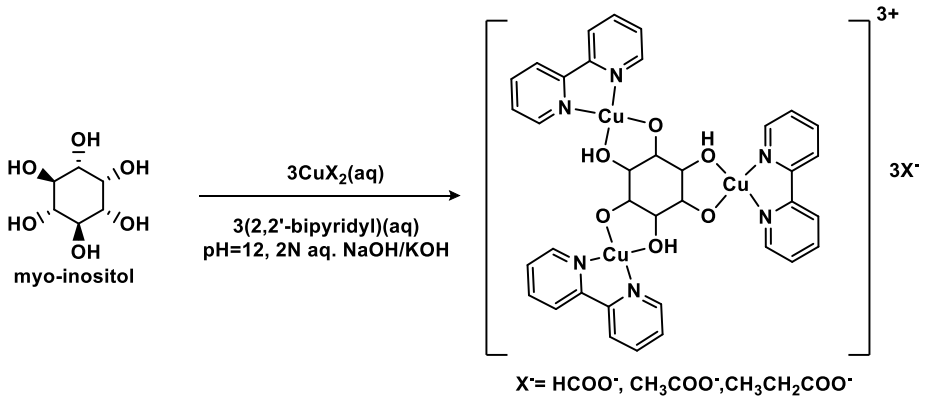

Scheme 2.2.2.1 Synthesis of the trinuclear Copper (II) complex hydrogelator.

Table 2.2.2.1 Codes and Composition of the metallogels		
Code	Counter Anion	Base
111	Formate	NaOH
121	Formate	KOH
121	Acetate	NaOH
122	Acetate	KOH
113	Propionate	NaOH
123	Propionate	KOH

2.2.3 Instrumentation and Techniques

UV-Visible: Perkin Elmer Lambda 35 dual beam UV–vis Spectrophotometer was used to record the spectra of metallogels, to monitor the pH dependence of gel formation and sol-gel transformation.

T_{gel}: Sol-gel transition temperature, T_{gel}, of the gels was measured using a Julabo 5 A thermostat with a temperature controller and a thermometer with an accuracy of ±0.05 $^{\circ}$C. Gels were taken in screw capped glass vials and immersed in a water bath whose temperature was gradually increased by a temperature control program and the T_{gel} temperatures were recorded using the inverted test-tube method.

TG–DTA: TG–DTA of the gels and xerogels was recorded using an SII TG/ DTA6300 EXSTAR instrument. The thermograms were recorded using a platinum pan in the temperature range from room temperature to 550°C for gels and up to 750°C for xerogels under an inert nitrogen atmosphere.

FTIR: FTIR spectra of xerogels were recorded using a PerkinElmer (Model: RX1) spectrometer in the form of KBr pellets.

Mass spectrometry: The ESI mass spectra of the hydrogels were recorded using a Waters UPLC-TCD or a Maxis Impact (Bruker) and an Applied Biosystem API 200 mass spectrometer.

NMR: The ^{1}H NMR spectra were recorded using a Bruker Avance 400 MHz instrument.

Computational Studies: Full geometry optimizations were carried out using density functional theory (DFT) with B3LYP[29–32] and LANL2DZ[33,34] basis set. Gaussian 16[35] and Gauss View 6[36] programs for computation and visualization of output.

Scanning electron microscopy (SEM): SEM analysis was performed using a JEOL JSM-5610 instrument. Xerogels were prepared on SEM stubs for capturing the SEM images.

Polarizing optical microscopy (POM): POM analysis was performed using a LEICADM2500P polarizing microscope. Images were captured using a LEICADFC295 camera, which is attached to the instrument. Images were processed using the software LAS V4.1. A thin layer of gel was formed on a glass slide and allowed to dry and get converted to a xerogel whose images were captured at various magnifications and different angles of the polarizer.

Rheology: The rheology studies of the metallo-hydrogels were performed using a TA Instruments ARES G2 rheometer. Amplitude sweep was performed at room temperature using 25 mm parallel plates.

2.3. Results and Discussion

The metallogelator complex, **$[Cu_3(H_3ins)(bipy)_3]X_3$** was prepared using three different methods. $CuX_2.H_2O$, 2,2'-bipyridine and myo-inositol were allowed to react in 3:3:1 molar ratio at pH 12 adjusted using NaOH or KOH as alkali. The $CuX_2.H_2O$ salts are cupric formate, cupric acetate and cupric propionate, respectively, with X = $HCOO^-$, CH_3COO^- and $CH_3CH_2COO^-$ **(Scheme 2.2.2.1)**.

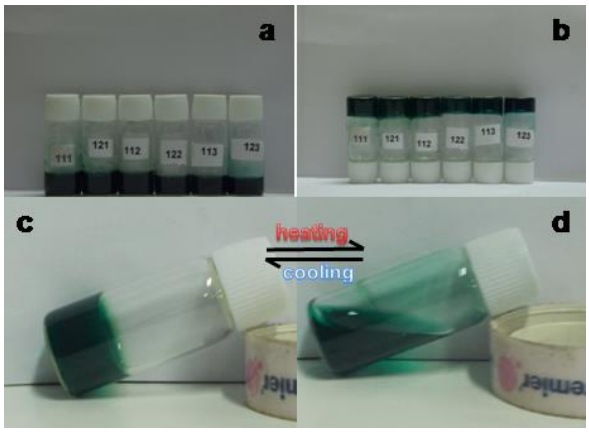

Figure 2.3.1 [a] Gels formed by the trinuclear Copper(II) complexes with myo-inositol, [b] Image of inverted vials which proves gel formation, [c]-gel and [d]-solution shows the sol-gel transformation on thermal stimuli.

Gelation was confirmed by inverted test tube-tube method **(Figure 2.3.1).** Composition of gels synthesized using different Copper(II) salts and alkali is detailed in **Table 2.2.2.1.**

2.3.1 UV-Visible spectroscopy:

As discussed previously, in the synthesis **Scheme 2.2.2.1**, the trinuclear copper (II) complex is formed by reaction of copper salts with 2,2'-bipyridine and myo-inositol. Presence of alkali ensured the deprotonation of myo-inositol and consequently the formation of the complex **$[Cu_3(H_3ins)(bipy)_3]^{3+}$**. The ternary complex along with the alkali formed the supramolecular assembly resulting into a metallogel. The change in the coordination sphere of metal center was confirmed by doing UV-Visible spectroscopy as discussed in **Figure 2.3.1** It was seen that there is a shift in the λ_{max} from a blue-coloured gel forming copper complex showing absorption at 662 nm to a green-coloured gel having an absorption maximum at 678 nm. In the metallogels reported here, the copper(II) center is coordinated to bipy and myo-inositol. The coordination of myo-inositol takes place in alkaline pH of 12, in presence of hydroxide base, after heating as mentioned in **Scheme 2.2.2.1**. The shift in the λ_{max} is a result of a change in the coordination sphere of the metal center due to the formation of supramolecular assembly.

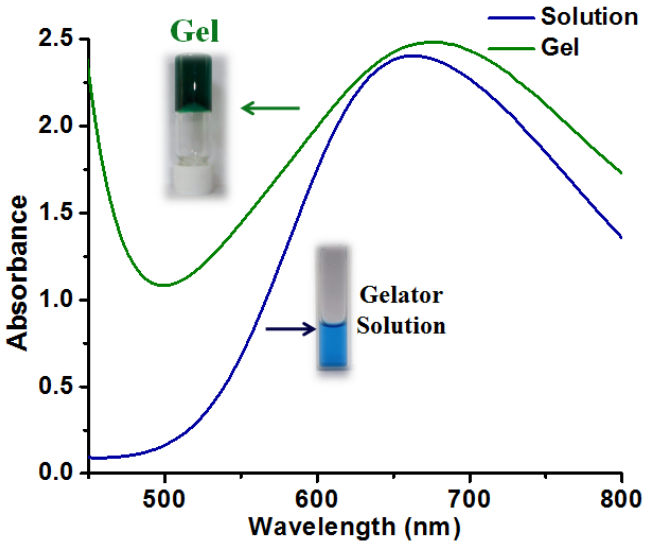

Figure 2.3.1.1 The UV-visible spectra during the sol-gel transformation during the metallogel formation.

2.3.2 Sol-Gel Transition temperature (T_{gel})

Gels are a heterogeneous system formed by an immobile network of the solid incorporating a mobile solvent. Consequently, the gels possess a solid like property that can sustain shear stress, which varies from system to system. At the gelation point an infinite cluster is created that spans the whole system and the system assembles into a gel having solid like property. The gelator systems are sensitive to temperature changes. When the gels are subjected to an elevated temperature the macroscopic properties change abruptly from solid like to liquid like property. The temperature, at which this transformation of the gel to a solution like behavior occurs, is called Sol-Gel temperature, also referred to as T_{gel}.[1]

The formation of the gels is characterized by inverted vial experiment **(Figure 2.3.1)** and T_{gel} temperature. The metallogels reported in this chapter were susceptible to thermal changes and T_{gel} temperatures were recorded for all the gels reported. The metallogels as mentioned in the **Scheme 2.2.2.1** were synthesized in presence of NaOH or KOH as alkali, the counter anions which are alkyl carboxylates were also varied in the synthesis of the gels. The effect of the variation in these parameters on the T_{gel} of the gels have been recorded and listed in **Table 2.3.2.1.**

Table 2.3.2.1 Optimum water retention capacity and the T_{gel} values of the metallohydrogels.

Gel codes	Optimum-water retention capacity per 100 mg of xerogel	T_{gel} (°C)
111	1.90 mL	41.5 ± 0.5
121	1.98 mL	39.5 ± 0.5
112	2.22 mL	46.0 ± 0.5
122	2.07 mL	43.5 ± 0.5
113	2.02 mL	49.0 ± 0.5
123	1.90 mL	45.5 ± 0.5

Though the cation, i.e., sodium or potassium, in the alkali used for maintaining the pH appears to have negligible effect, the gels prepared using NaOH as a base have slightly higher T_{gel} values than the gels prepared using KOH. The carboxylate anions, however, do have a significant effect on the gel properties. This can be seen in a gradual increase in the T_{gel} values measured by inverted test tube method using a JULABO 5A thermostat with a temperature programmer. As seen from the **Table 2.3.2.1** the T_{gel}

gradually increases as the alkyl chain of the counter anion increases from formate to acetate to propionate in the corresponding gels.

2.3.3 Thermogravimetric analysis of gels and xerogels

The hydrogels formed by the trinuclear copper(II) complexes immobilize water as a solvent. The TGA of the gels as well as xerogel was performed in platinum pan, the TGA of the gels gave information about the optimum water uptake capacity of the gels **(Table 2.3.2.1)**, while the TGA of the xerogel throws light on the binding present in the trinuclear copper(II) complex. The TGA of xerogel was also done with the purpose of finding the thermal stability of the gelator complexes.

All six gels were found to absorb 1.90 to 2.22 mL water per 100 mg of the xerogel **(Table 2.3.2.1).** In the thermograms of the xerogels, mass loss corresponding to the water molecules was observed which is followed by a loss of carboxylate moiety. Mass loss centered at 200°C to 225 °C corresponds to the loss of bipy while further mass loss was because of inositol moiety. The mass loss corresponding to bipy and inositol is usually observed at ~159°C and ~375°C, respectively. However, in the xerogels these fragments were found to be lost between the temperature ranges ~160°C-300°C and ~300°C - 550°C. The increase in the temperature indicates chemical interaction of bipy and inositol, thus supporting the involvement of these molecules in coordination with copper(II). It was observed from the TG-DTA of the xerogels that the relative mass loss of bipy : inositol in this region was in the ratio of ~2.6:1 corresponding to the molar ratio of bipy : inositol = 3 : 1 as present in the metallogelator trinuclear complex. Similar observation was made in the thermograms of all six gels and corresponding xerogels represented in the thermograms given below (**Figure 2.3.3.7** to **Figure 2.3.3.12**). The higher temperature for loss of inositol moiety due to its interaction with the metal center also supports the formation of a ternary trinuclear complex which is the actual gelator molecule.

TG- DTA of gels

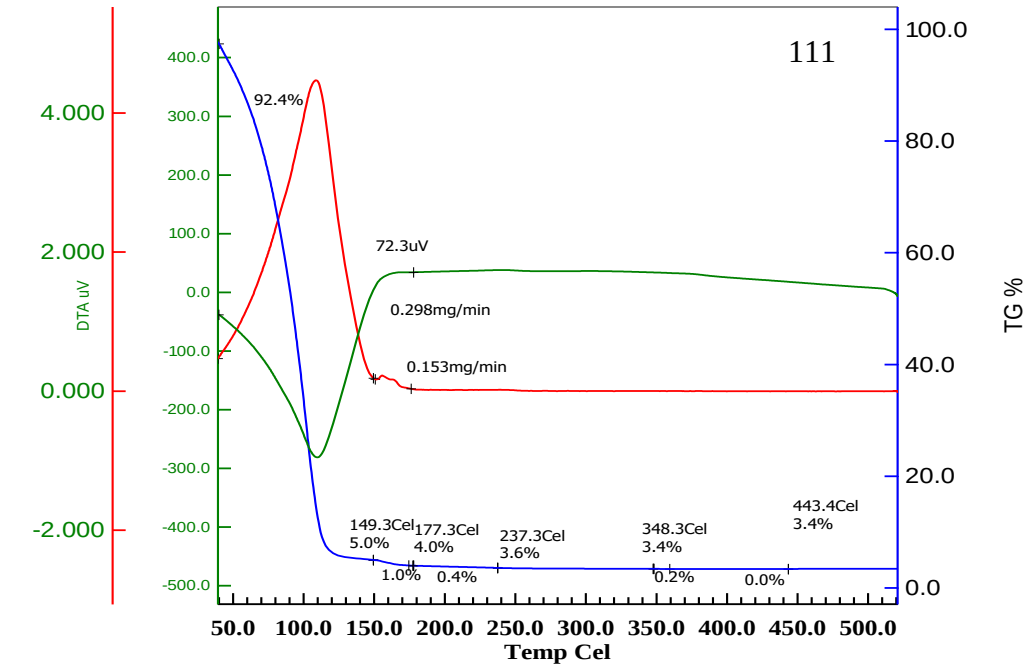

Figure 2.3.3.1 TG-DTA of gel 111.

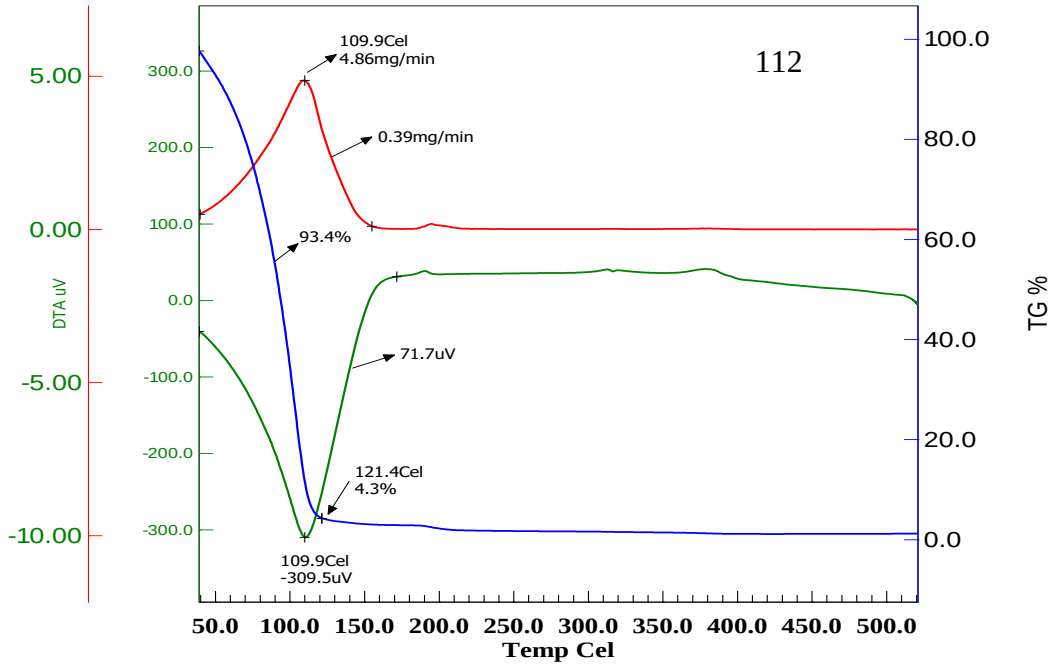

Figure 2.3.3.2 TG-DTA of gel 112.

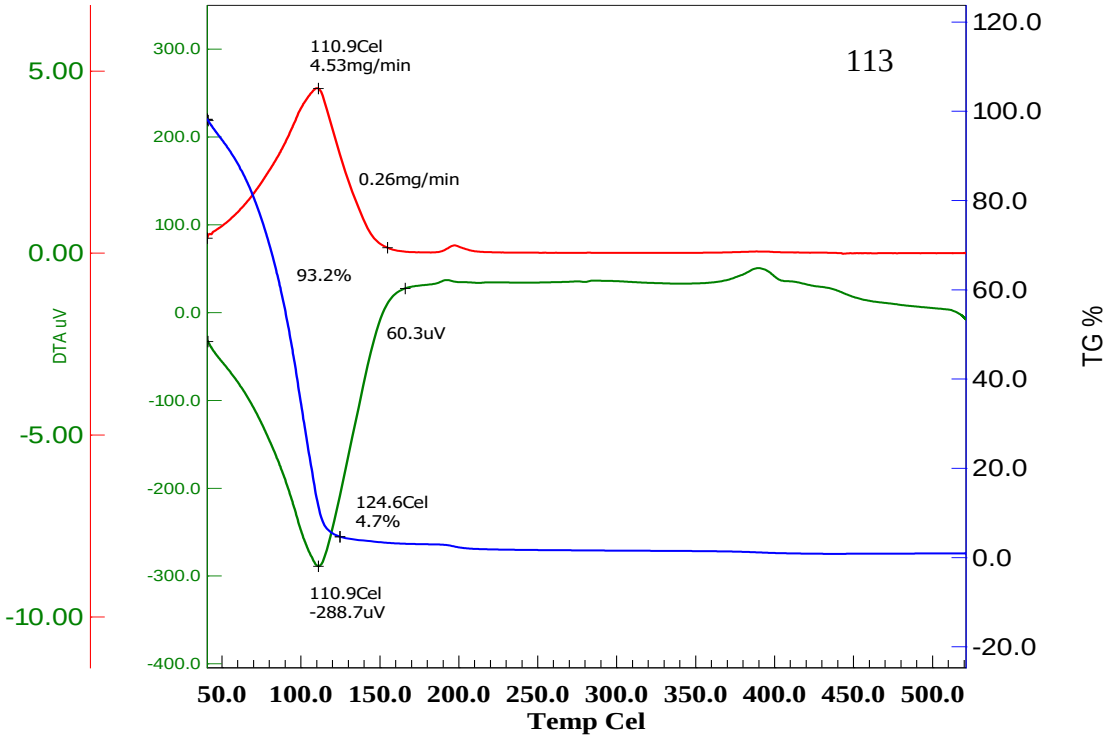

Figure 2.3.3.3 TG-DTA of gel 113

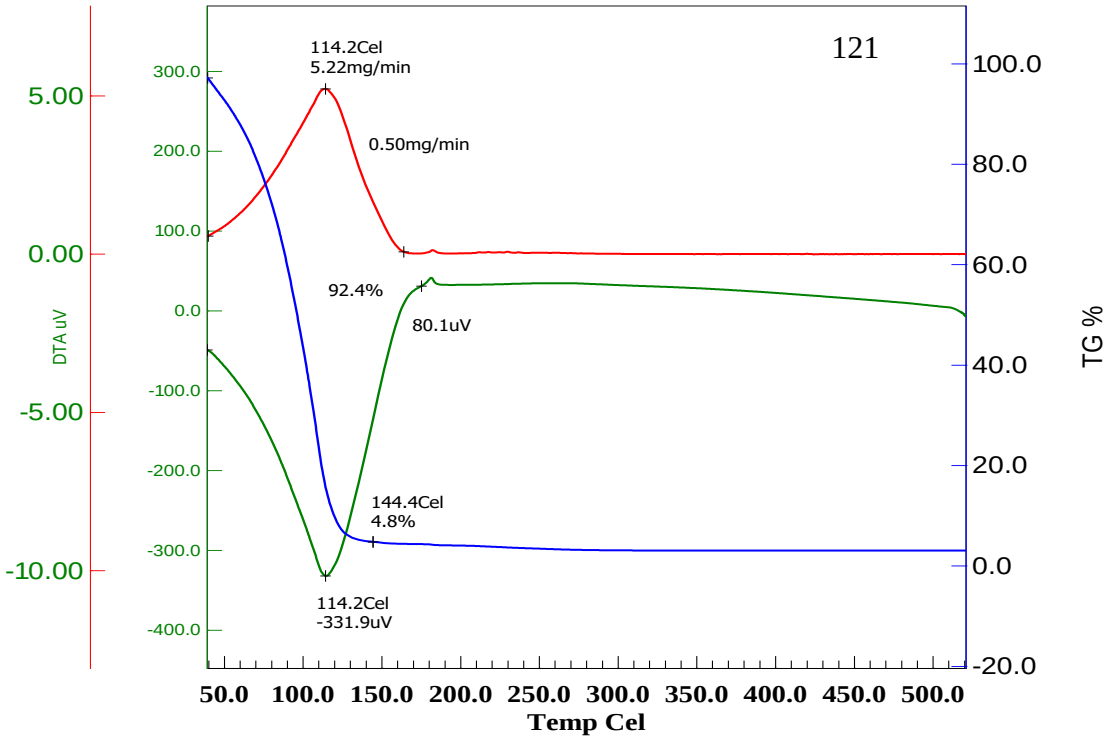

Figure 2.3.3.4 TG-DTA of gel 121

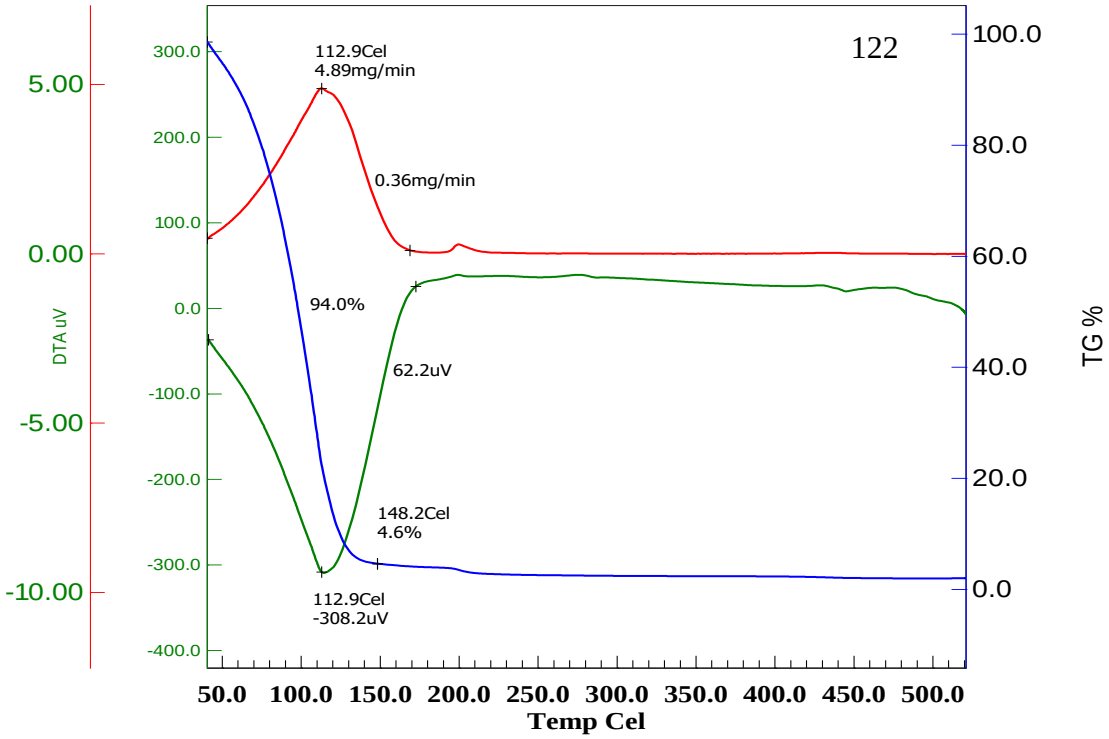

Figure 2.3.3.5 TG-DTA of gel 122

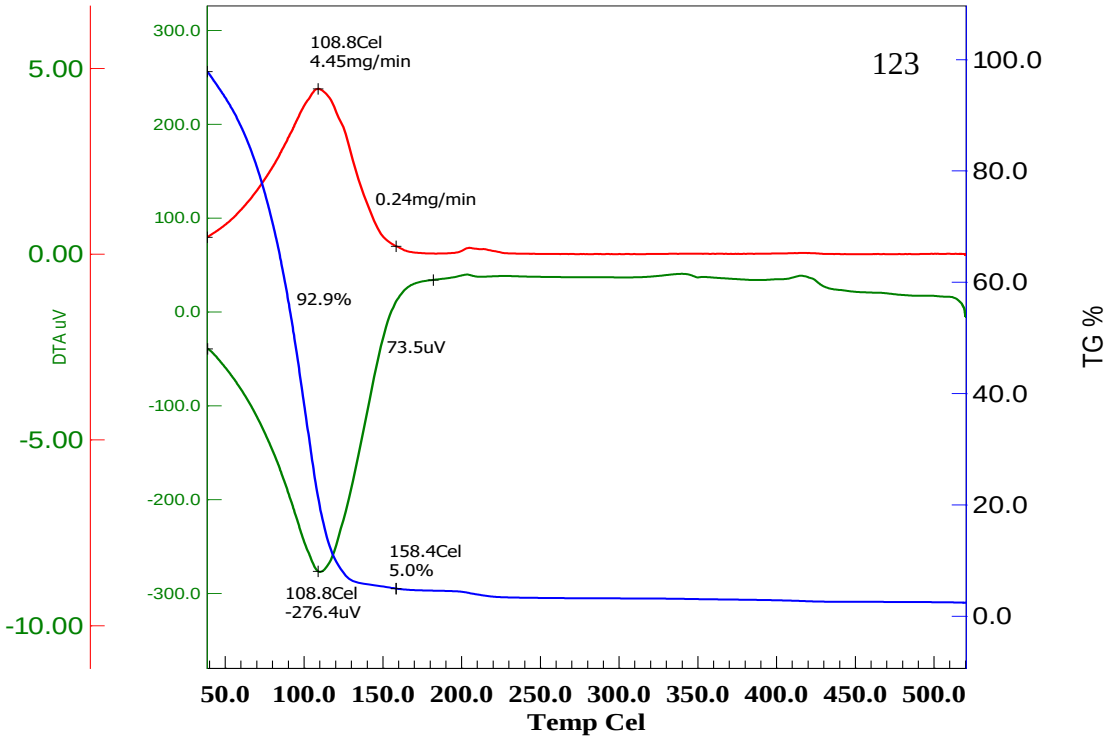

Figure 2.3.3.6 TG-DTA of gel 123

TG- DTA of xerogels

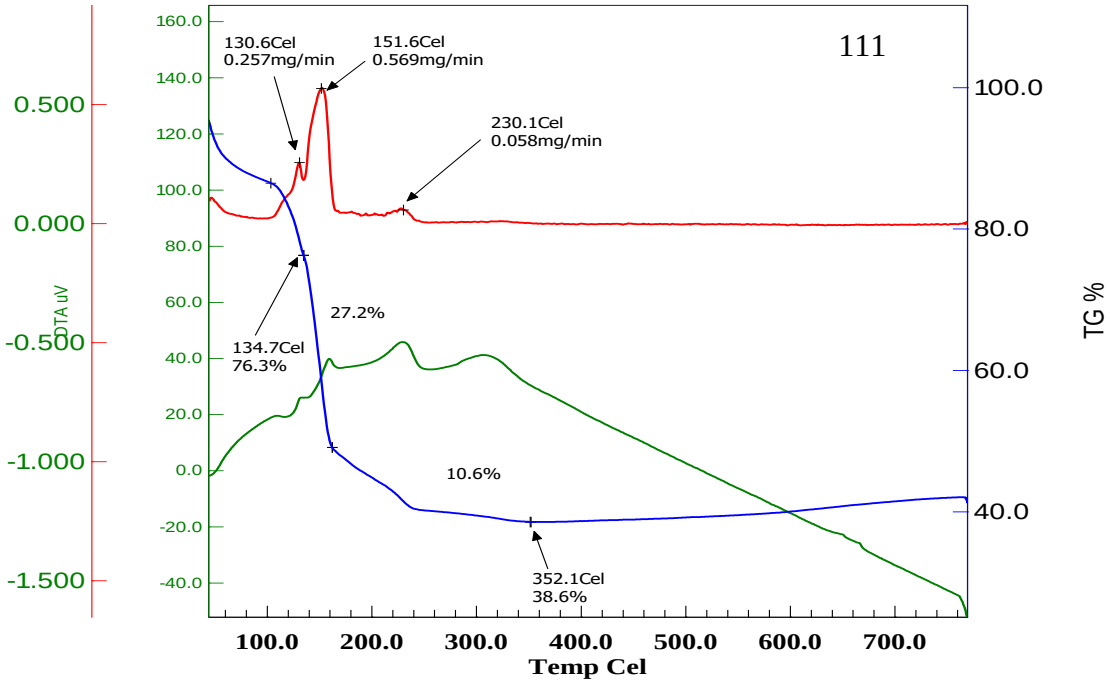

Figure 2.3.3.7 TG-DTA of xerogel 111

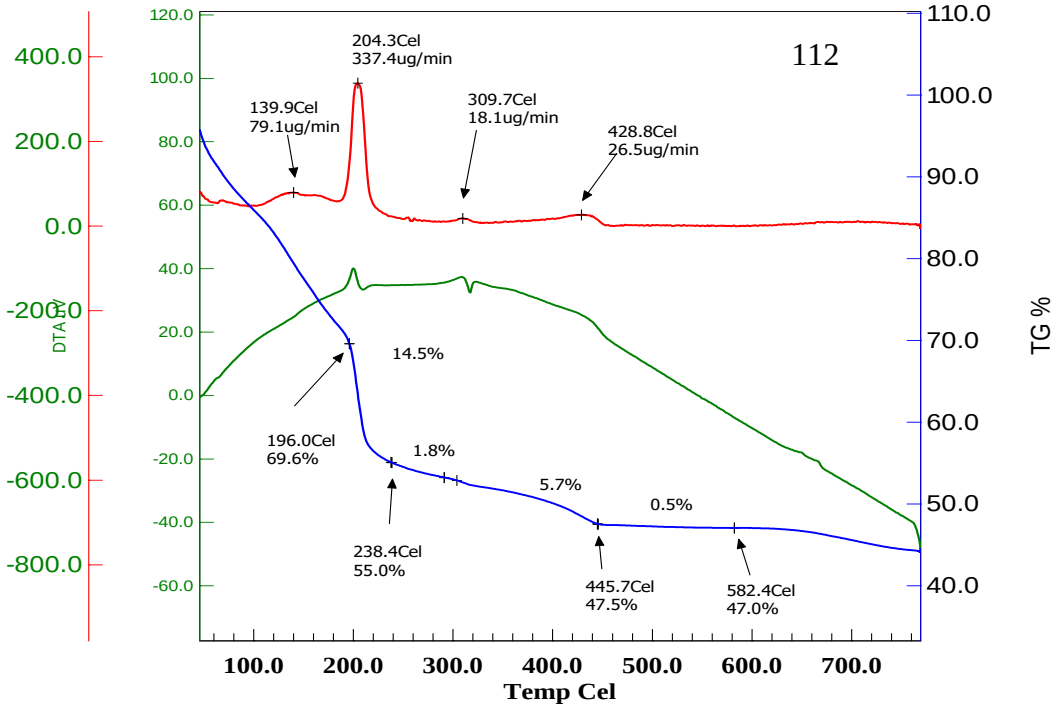

Figure 2.3.3.8 TG-DTA of xerogel 112

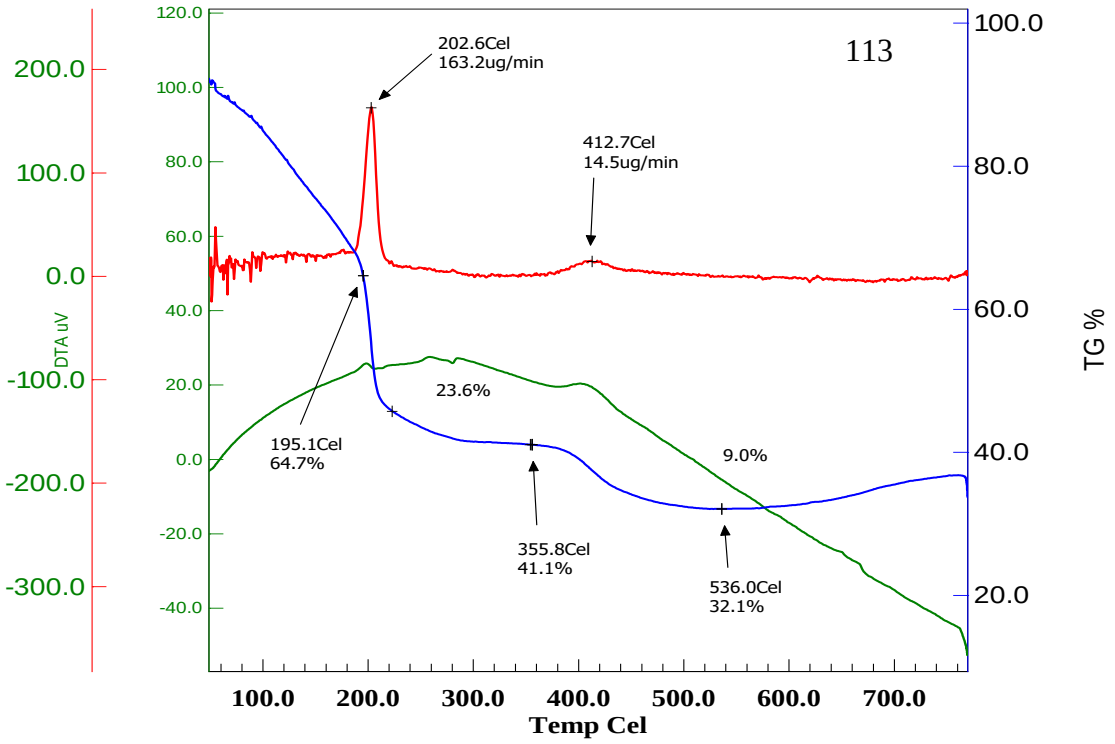

Figure 2.3.3.9 TG-DTA of xerogel 113

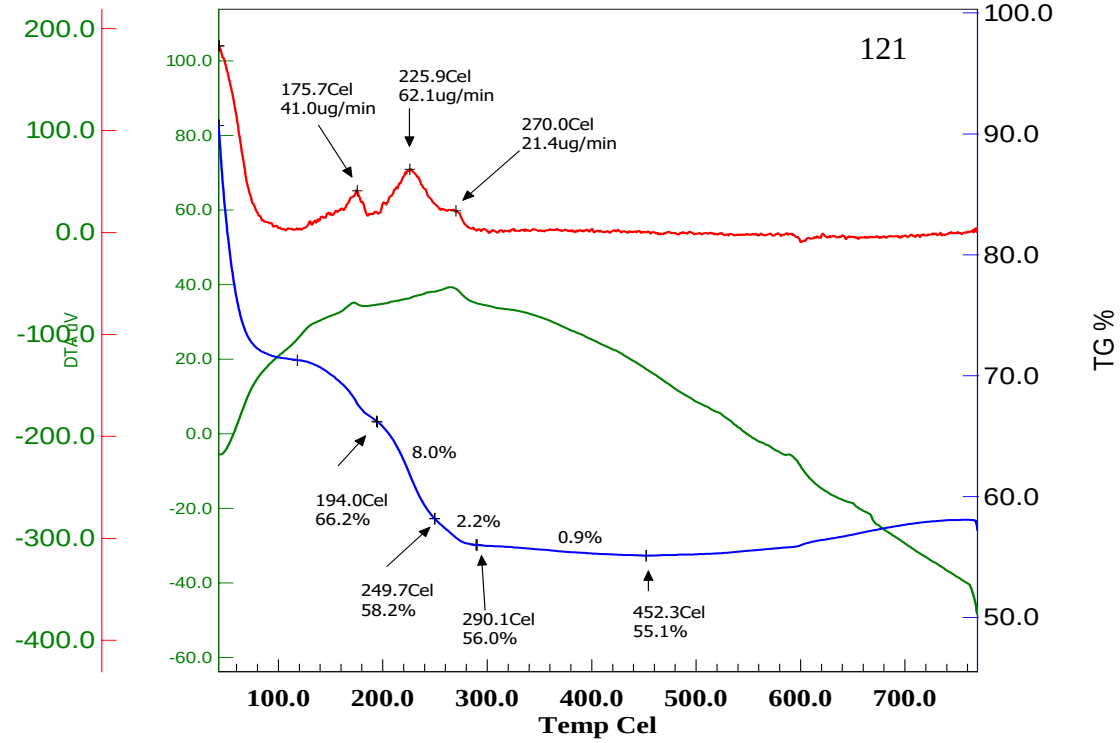

Figure 2.3.3.10 TG-DTA of xerogel 121

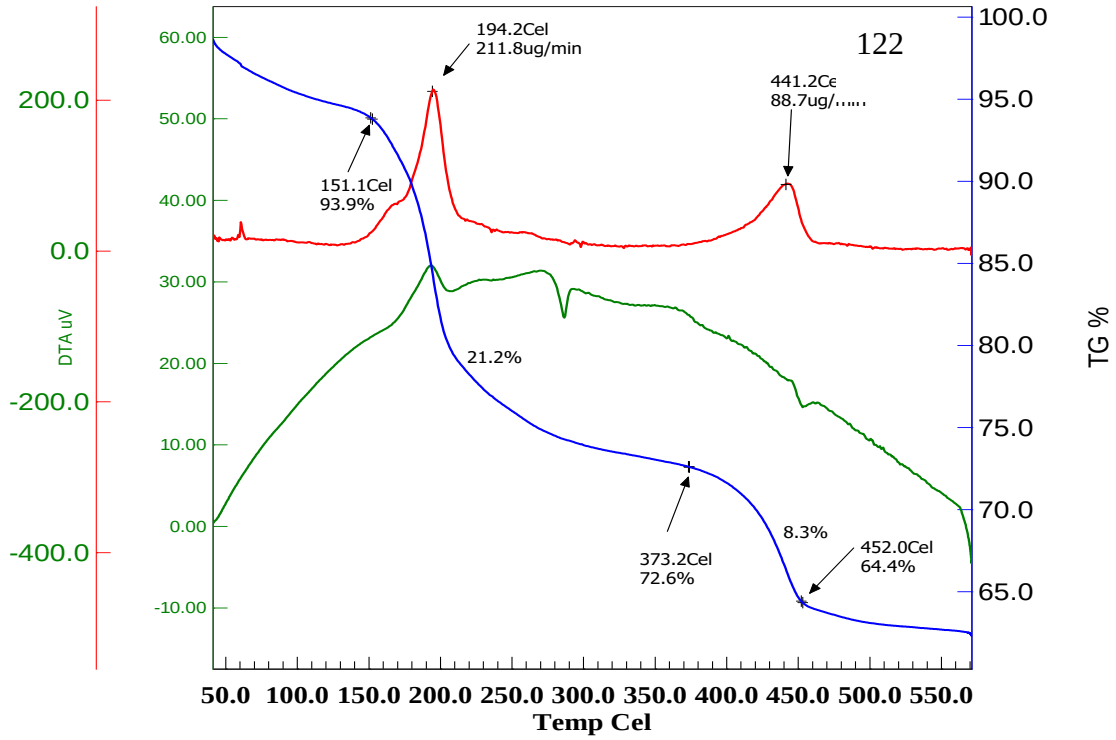

Figure 2.3.3.11 TG-DTA of xerogel 122

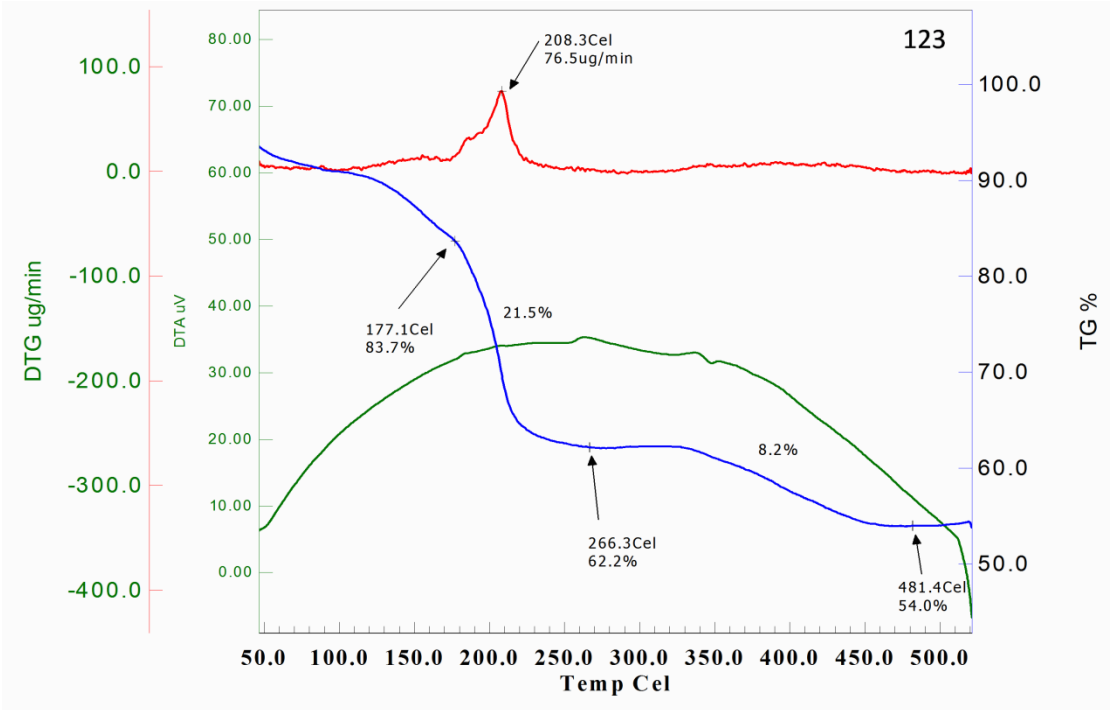

Figure 2.3.3.12 TG-DTA of xerogel 123

2.3.4 FTIR Spectra of Xerogels

The metallo-hydrogels were dried and converted to the respective xerogels in order to record their FTIR spectra. The FTIR spectra recorded in the form of KBr pellets of xerogels exhibited important bands corresponding to the vibrations in both myo-inositol and bipy. Among these, the aliphatic C-H stretching vibrations at 2700-3000 cm^{-1}, the C-C multiple bond stretching and the ring C-N vibration in bipy between 1400-1700 cm^{-1} were prominent. The presence of absorption bands at ~1030, 900 and 770 cm^{-1} supported the coordination of bipy while the absorptions at ~1100, 730 and 660 cm^{-1} supported the presence of coordinated inositol **(Figure 2.3.4.1 to Figure 2.3.4.6)**. The xerogels were washed with ethanol followed by water to remove free bipy, copper acetate and binary complexes if any formed during the reaction as these were freely soluble. Thus, the residue obtained after washing was expected to be the corresponding ternary complex **$[Cu_3(H_3ins)(bipy)_3]X_3$**, where X = a carboxylate. As the ternary complex ion present in the xerogel remained the same, the FT-IR spectra of the xerogels resemble with each other and show the prominent vibrations as discussed above. As the counter anions were varied during the study the vibrations corresponding to the counter anions namely formate, acetate and propionate were different amongst the xerogels discussed.

FT-IR data for xerogels:

Xerogel-111: FT-IR, cm^{-1} (KBr): 3425.96, 2887.88 2822.90, 2718.15, 1598.15, 1472.96, 1444.70, 1393.88, 1352.20,1161.20, 1103.18, 1030.16, 951.44, 898.09, 770.70, 732.09, 662.63, 588.81, 514.76

Xerogel-121: FT-IR, cm^{-1} (KBr): 3409.85, 2811.16, 2723.06, 1591.21, 1495.17, 1474.88, 1445.78, 1349.33, 1162.16, 1105.52, 1030.24, 899.10, 771.76, 732.21, 586.04

Xerogel-112: FT-IR, cm^{-1} (KBr): 3437.18, 2833.42, 1641.03, 1562.35, 1412.50, 1335.71, 1247.33, 1161.52, 1106.70, 1022.77, 927.59, 895.91, 777.93, 642.85, 519.06

Xerogel-122: FT-IR, cm^{-1} (KBr): 3469.66, 3282.38, 3163.29, 2982.19, 1707.18, 1641.55, 1568.17, 1413.91, 1337.56, 1245.68, 1159.66, 1119.49, 1051.89, 1019.90, 926.56, 781.30, 644.48, 520.38

Xerogel-113: FT-IR, cm^{-1} (KBr): 3435.29, 2972.93, 2938.73, 2874.27, 2833.04, 1684.08, 1642.04, 1563.63, 1464.48, 1427.36, 1369.42, 1334.22, 1297.02, 1159.89, 1076.07, 1029.63, 879.94, 814.85, 779.66, 730.68, 647.07, 508.24

Xerogel-123: FT-IR, cm^{-1} (KBr): 3410.56, 2976.46, 2884.48, 2826.61, 1666.71, 1564.30, 1471.10, 1410.73, 1366.44, 1297.62, 1162.13, 1077.22, 1027.76, 885.21, 774.81, 730.68, 654.68, 488.15

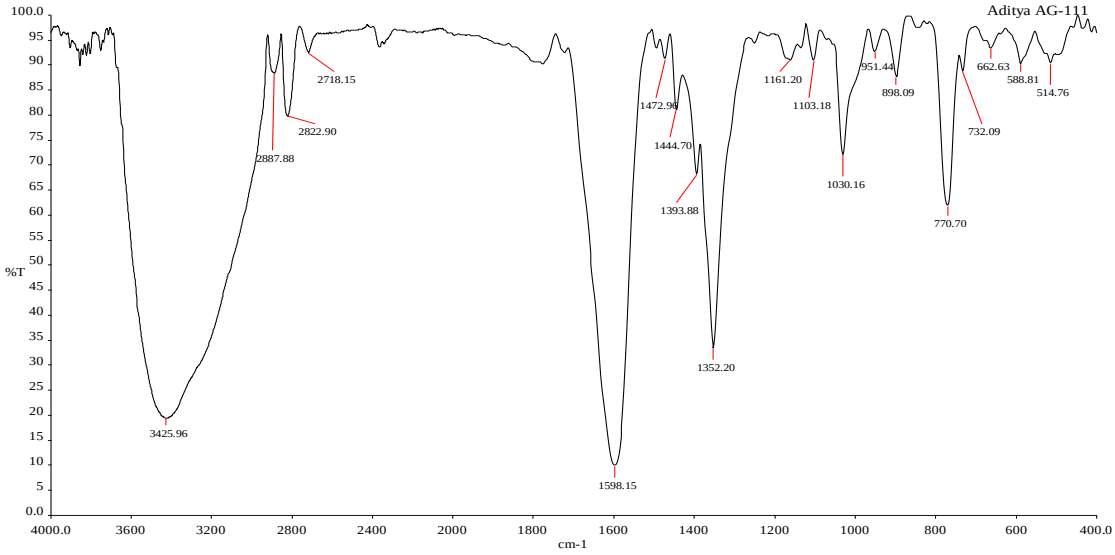

Figure 2.3.4.1 FTIR spectrum of xerogel 111.

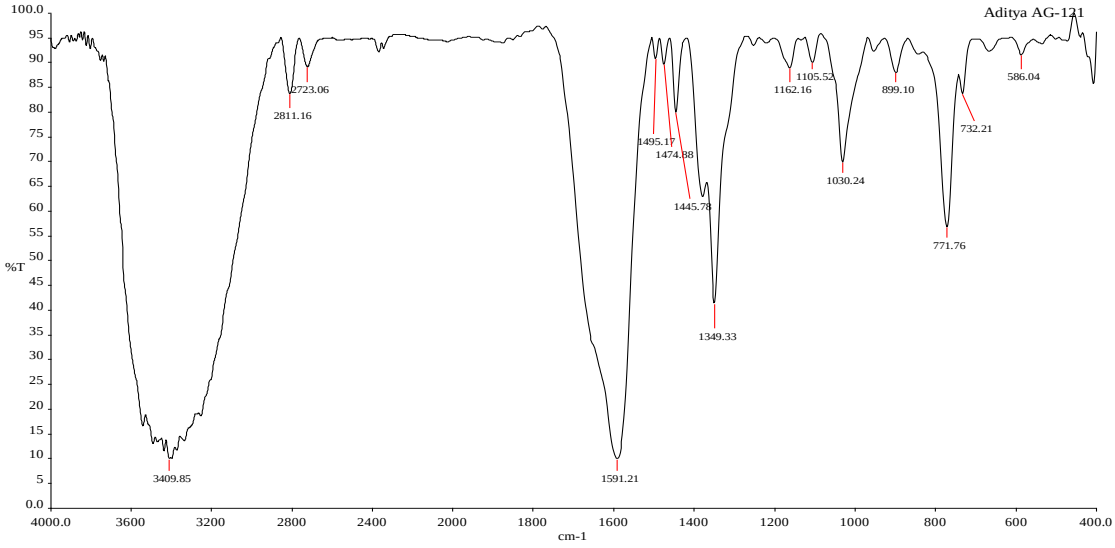

Figure 2.3.4.2 FTIR spectrum of xerogel 121.

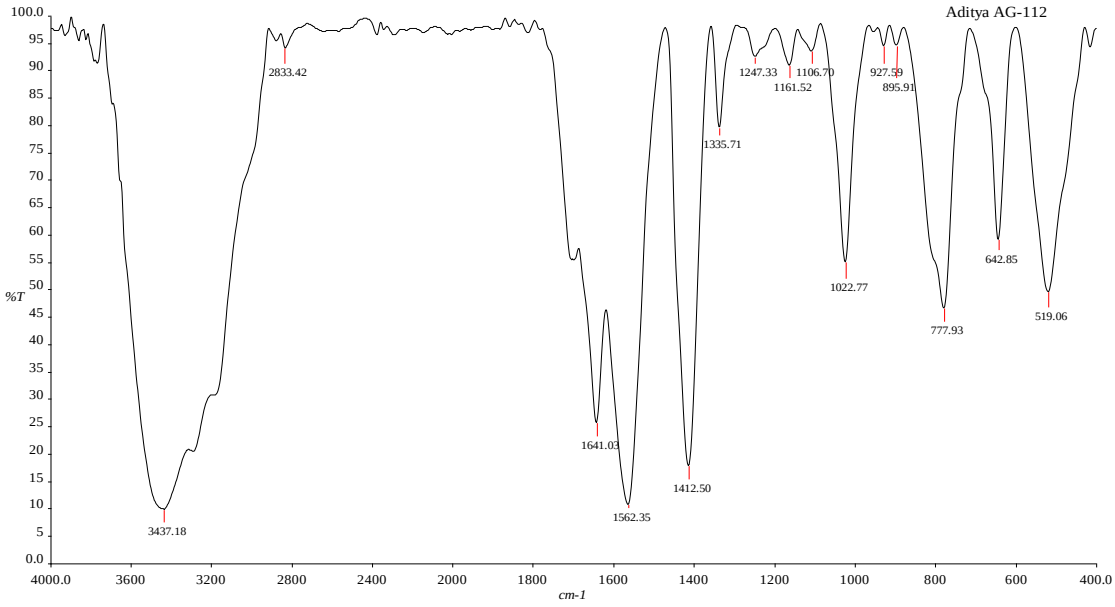

Figure 2.3.4.3 FTIR spectrum of xerogel 112.

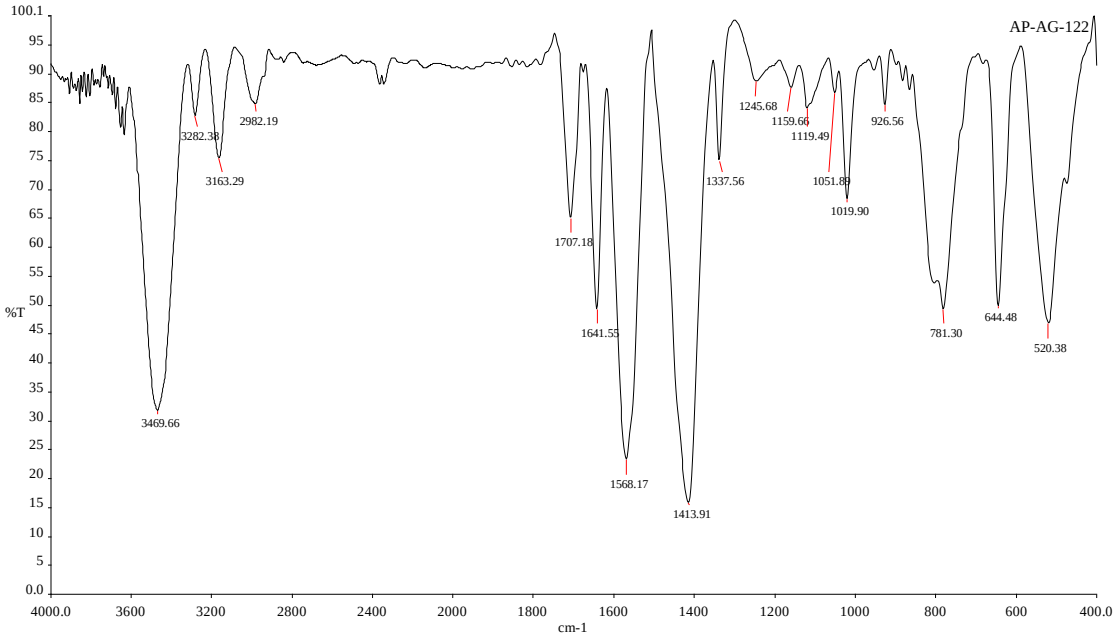

Figure 2.3.4.4 FTIR spectrum of xerogel 122.

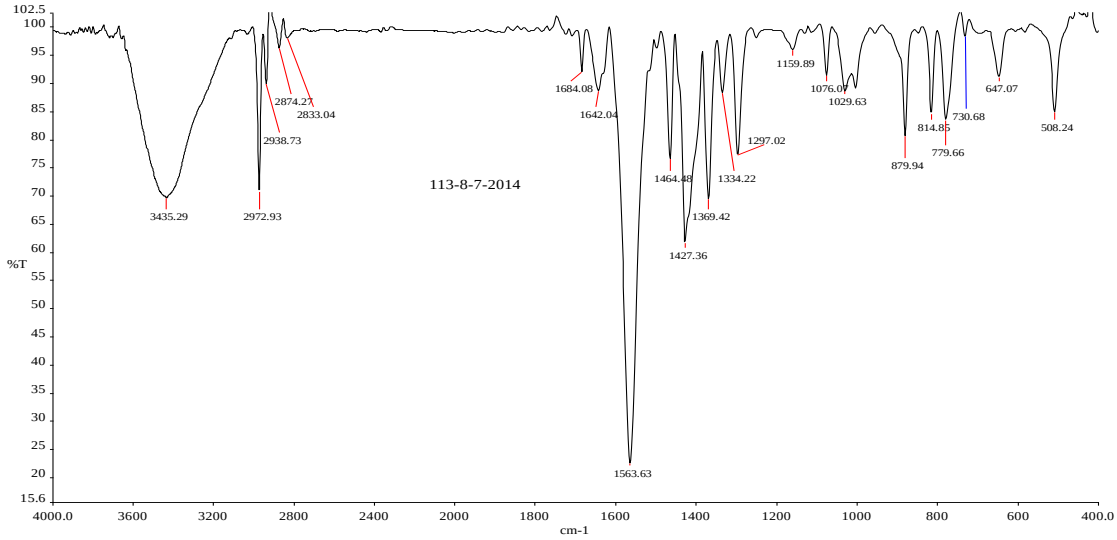

Figure 2.3.4.5 FTIR spectrum of xerogel 113.

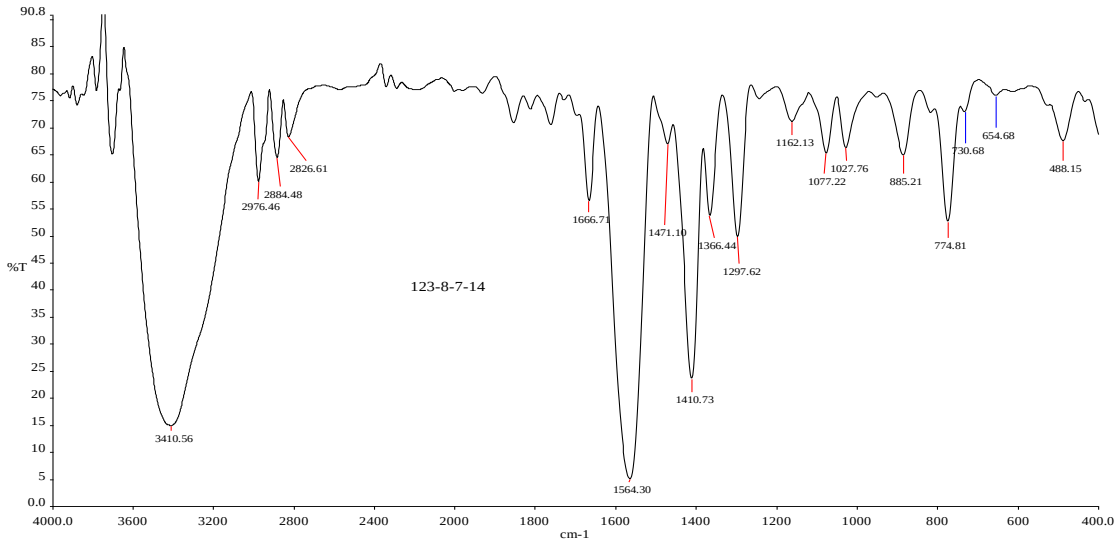

Figure 2.3.4.6 FTIR spectrum of xerogel 123.

2.3.5 ESI-MS Analysis of Metallogels

The gels were formed using copper salts and 2,2'-bipyridine (bipy) and myo-inositol as ligands. The supramolecular assemblies which result in the formation of the metallogels are formed because of the complex cation **$[Cu_3(H_3ins)(bipy)_3]^{3+}$**. In order to prove the existence of the complex ESI-MS spectroscopy of the metallogels was carried out. The ESI-MS of the gels (**Figure 2.3.5.1 to Figure 2.3.5.6)** recorded in aqueous media have prominent peaks corresponding to $[Cu(bipy)]^{2+}$ (m/z 218.95, 220.9) and $[Cu_3(H_3ins)(bipy)_3]^{3+}$ (m/z=277.95, 279.95). These are related to the isotopic abundance of copper with mass numbers 63 and 65 in 3:1 ratio. The peaks at m/z=277.95, 279.95 have been in the mass spectra of all gels. This supports the existence of trinuclear trication, $[Cu_3(H_3ins)(bipy)_3]^{3+}$, in the gels which must be further undergoing H-bond formation or coordination with water molecules. In the basic medium the hydroxide must be participating in the hydrogen bonded assembly along with the anions - formate, acetate and propionate - present as counter anions.

Table 2.3.5.1 Table showing the fragments observed in the ESI-MS

Fragments	m/z values
$[Cu_3(H_3ins)(bipy)_3]^{3+}$	**278**
$[Cu(bipy)]^{2+}$	**219**
$[Cu(bipy)_2]^{+}$	**375**

As only the counter anions X^- (formate, acetate and propionate) and alkali (NaOH or KOH) were changed in the metallogel synthesis, trinuclear trication, $[Cu_3(H_3ins)(bipy)_3]^{3+}$ responsible for the formation of metallogels remained same in all the metallogels. The peaks m/z=277.95, 279.95 that correspond to the trinuclear trication, $[Cu_3(H_3ins)(bipy)_3]^{3+}$, were observed in the mass spectra of all the metallogels (**Figure 2.3.5.1 to Figure 2.3.5.6)**.

The m/z values of some of the species formed during the ESI-MS of the metallogels have been documented in the **Table 2.3.5.1.**

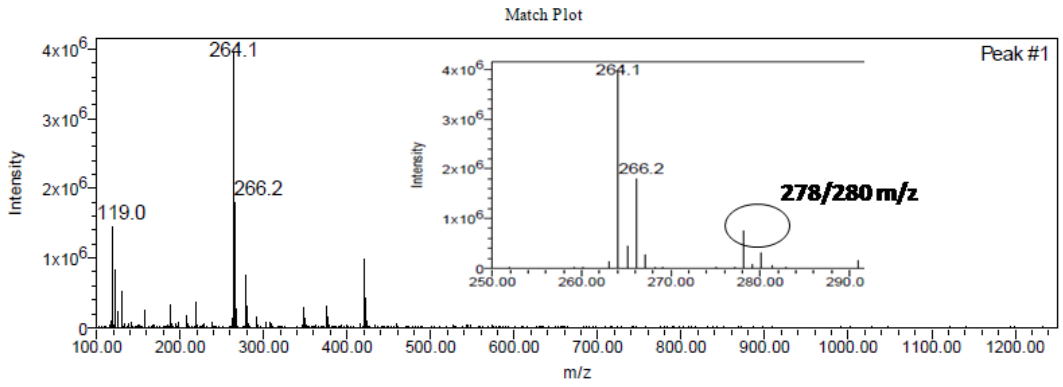

Figure 2.3.5.1 ESI-MS of the metallogel-111.

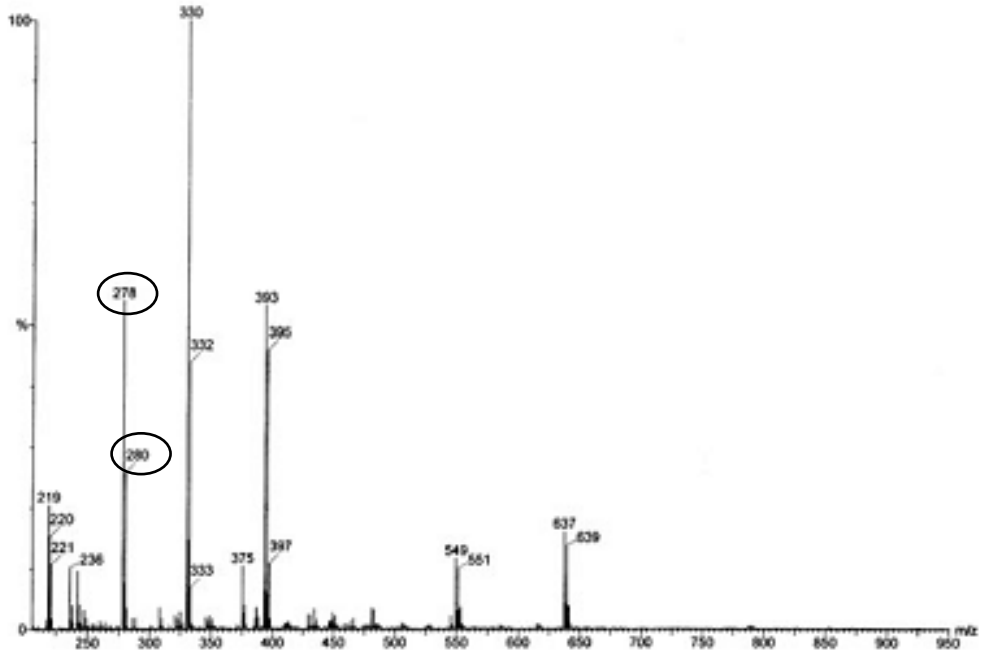

Figure 2.3.5.2 ESI-MS of the metallogel-112.

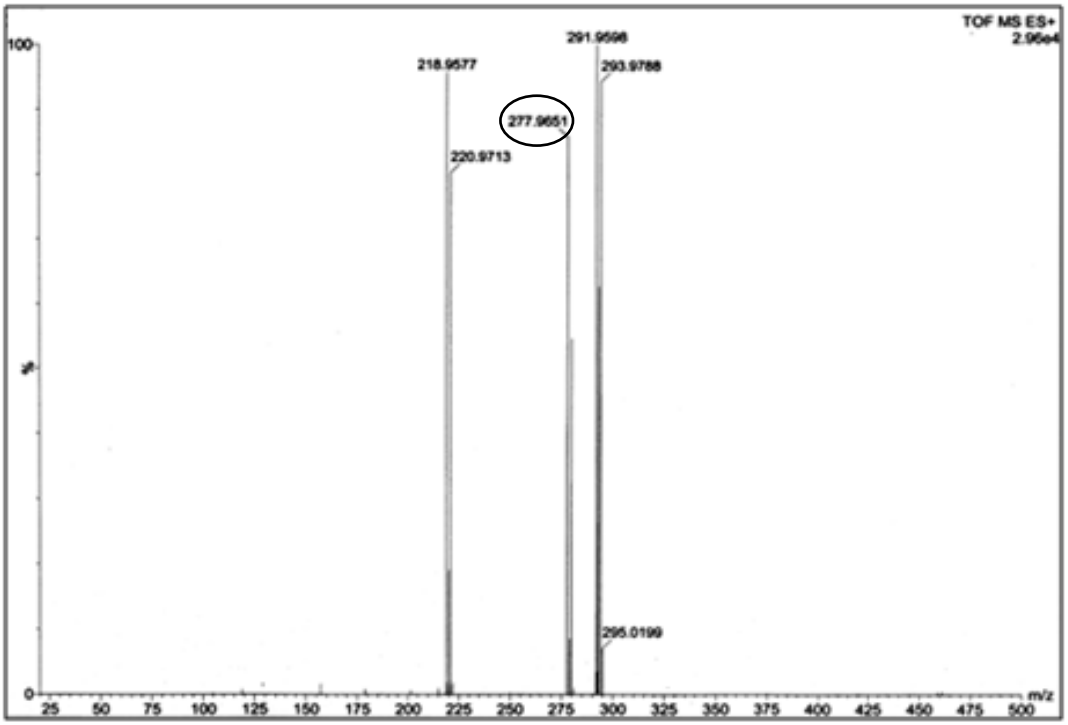

Figure 2.3.5.3 ESI-MS of the metallogel-113.

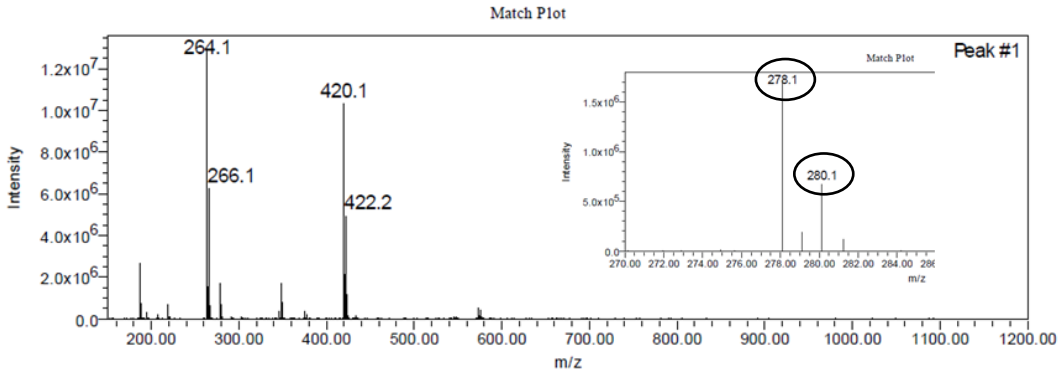

Figure 2.3.5.4 ESI-MS of the metallogel-121.

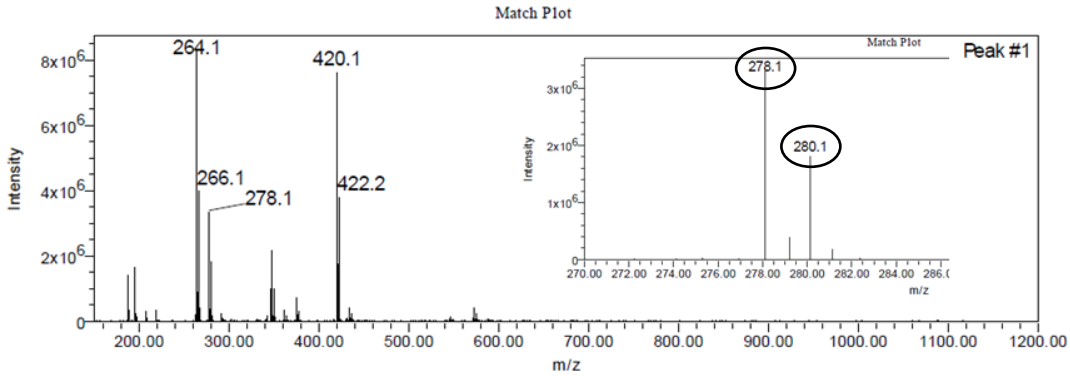

Figure 2.3.5.5 ESI-MS of the metallogel-122.

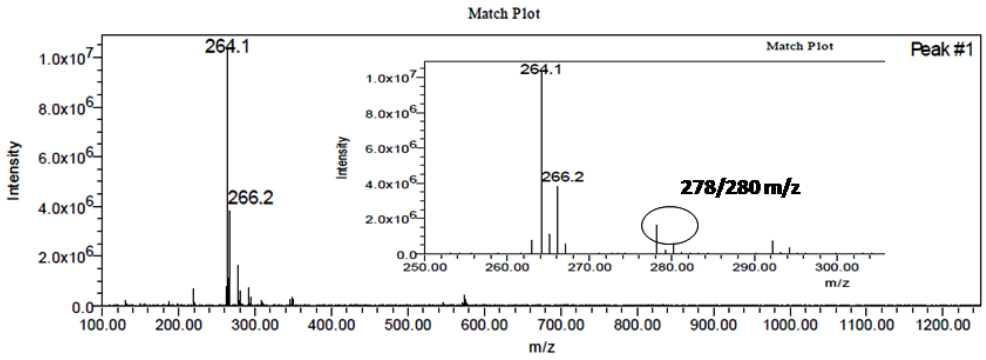

Figure 2.3.5.6 ESI-MS of the metallogel-123.

2.3.6 NMR spectral studies

The ^{1}H-NMR studies of inositol were carried out in order to verify the changes in inositol at higher pH values. ^{1}H NMR of free inositol in D_2O media was compared with that of the solution containing same equivalent of base (KOH) which is required for gel formation. The chemical shift values of various C-H protons, normalized with respect to deuterium lock are listed in **Table 2.3.6.1** As is evident from the Figure **2.3.6.1** as well as from the values in **Table 2.3.6.1**, the C-H protons of inositol shifted towards upfield values, though the splitting pattern remains exactly the same. This was an indication that inositol undergoes deprotonation at pH = 12, however the molecular backbone remains unchanged.

Table 2.3.6.1 Change in chemical shift values of myo-inosiol protons in presence of alkali.

Proton Label*	Chemical shift (δ) (inositol)**(A)**	Chemical shift (δ) (insoitol+KOH) **(B)**	Difference in δ values **(A-B)**
1	3.12	3.06	0.06
2	3.38	3.30	0.08
3	3.47	3.40	0.07
4	3.90	3.83	0.07

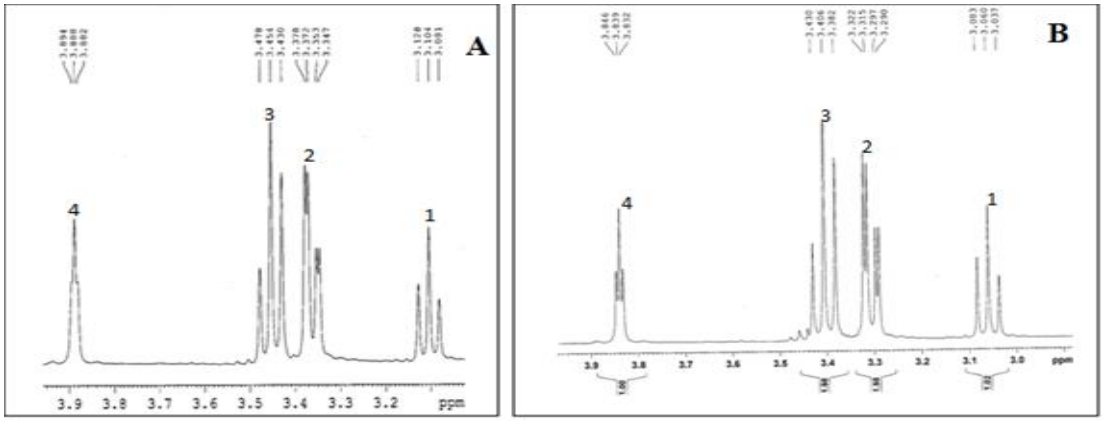

Figure 2.3.6.1 [A] ^{1}H NMR spectrum of inositol and [B] ^{1}H NMR spectrum of insoitol+base (KOH).

2.3.7 Structure of the complex cation and Computational studies

In order to get insights into the bonding and geometry of the trinuclear complex, the computational studiesc have been carried out.

FT-IR, ESI-MS and proton NMR studies supported the coordination of myo-inositol and formation of the ternary trinuclear gelator complex. There have been a few references citing the binding of myo-inositol to the metal centers.[37–40] In one such report Jinguang Wu et al[41] in 2013 reported a Cs^{+} complex where Cs^{+} is 10-coordinated to three chloride ions, O1 and O2 from one myo-inositol molecule, O3 and O4 from another myo-inositol molecule and O5 and O6 from the third myo-inositol molecule. This indicates that all six oxygen atoms of myo-inositol can participate in interaction with a metal ion.

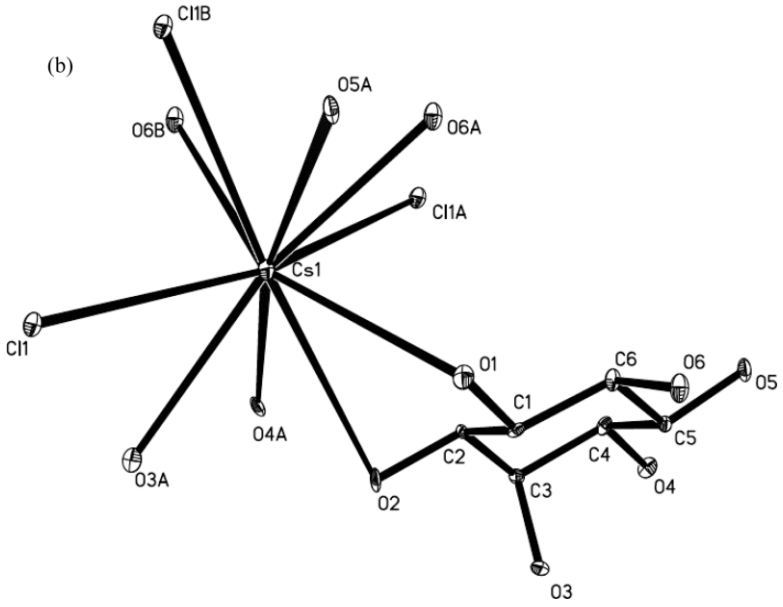

Figure 2.3.7.1 Crystal structure of CsCl−myo-inositol complexes (Image adapted with permission from reference[41] reported by Wu *et al* Copyright The American Chemical Society)

The complex cation **$[Cu_3(H_3ins)(bipy)_3]^{3+}$** is responsible for the metallogel formation, however, in spite of numerous attempts, the complex cation/molecule did not crystallize. As a result, the single crystal structure of the complex could not be determined.

To get an insight into the structure and bonding of the gels, an attempt has been made to theoretically model the complex ion by geometry optimization using DFT. The geometry of the complex cation, **$[Cu_3(H_3ins)(bipy)_3]^{3+}$**was optimized by DFT calculations using Gaussian 16 wherein B3LYP[29–32] and LanL2DZ[33,34] basis sets were used for the computation. **Figure 2.3.7.2** shows the optimized geometry of the complex, with Zero-point vibrational energy of 1717.206 KJoules/Mol (410.42218 Kcal/Mol). The Cu-N distances are found to be between 1.99 – 2.01 A^o, Cu-O bond distances of ~1.91 A^o and Cu-OH distances are between 2.05 - 2.1 A^o. All six oxygen atoms with Mulliken charges between -0.547and -0.604 are expected to be good electron donors and hence coordinate with the metal ions. The calculated bond distances are indeed within the range of coordinate bond lengths. The important geometrical parameters involving metal coordination are tabulated below (**Table 2.3.7.2).**

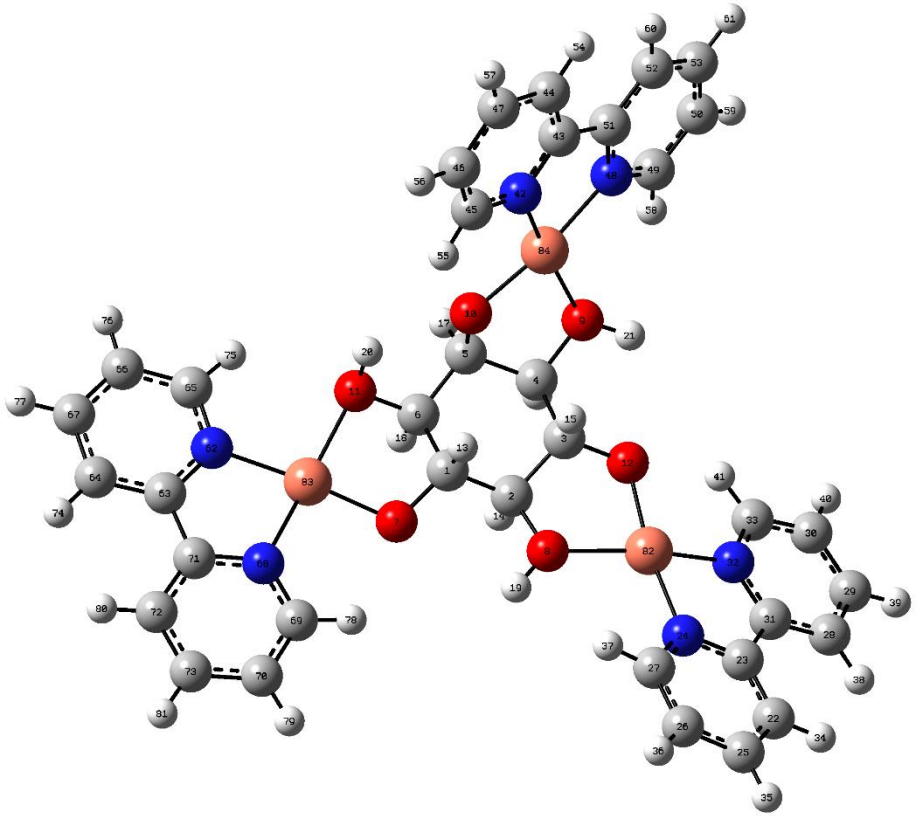

Figure 2.3.7.2 The optimized structure of the complex $[Cu_3(H_3ins)(bipy)_3]^{3+}$ using B3LYP theory and LanL2DZ as basis sets.

The Lowest Unoccupied Molecular Orbital (LUMO) and Highest Occupied Molecular Orbital (HOMO) acts as electron acceptor and electron donor.[42] Theoretical transition energy levels between HOMO and LUMO frontier molecular orbitals were calculated by B3LYP and LANL2DZ methods for the metallogelator complex **$[Cu_3(H_3ins)(bipy)_3]^{3+}$**and are tabulated in **Table 2.3.7.1.**

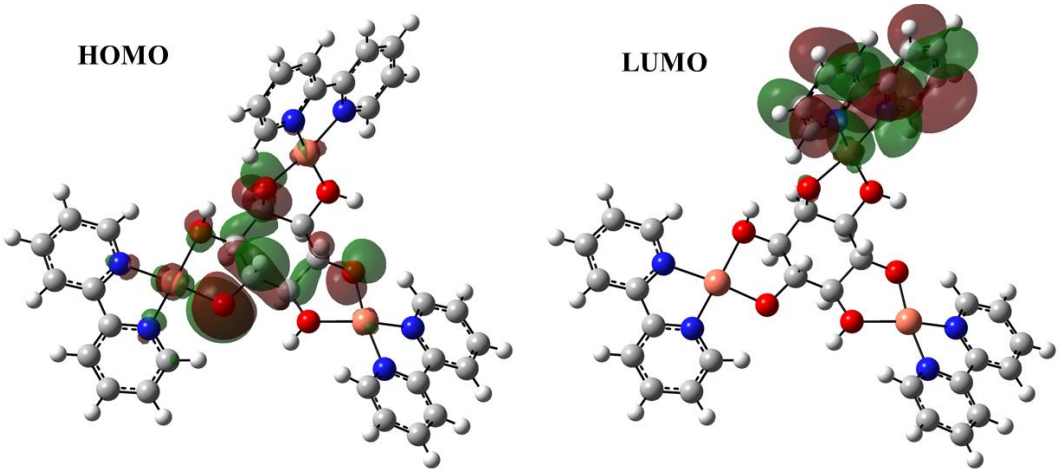

Figure 2.3.7.3 The HOMO and LUMO orbitals for the metallogelator complex $[Cu_3(H_3ins)(bipy)_3]^{3+}$.

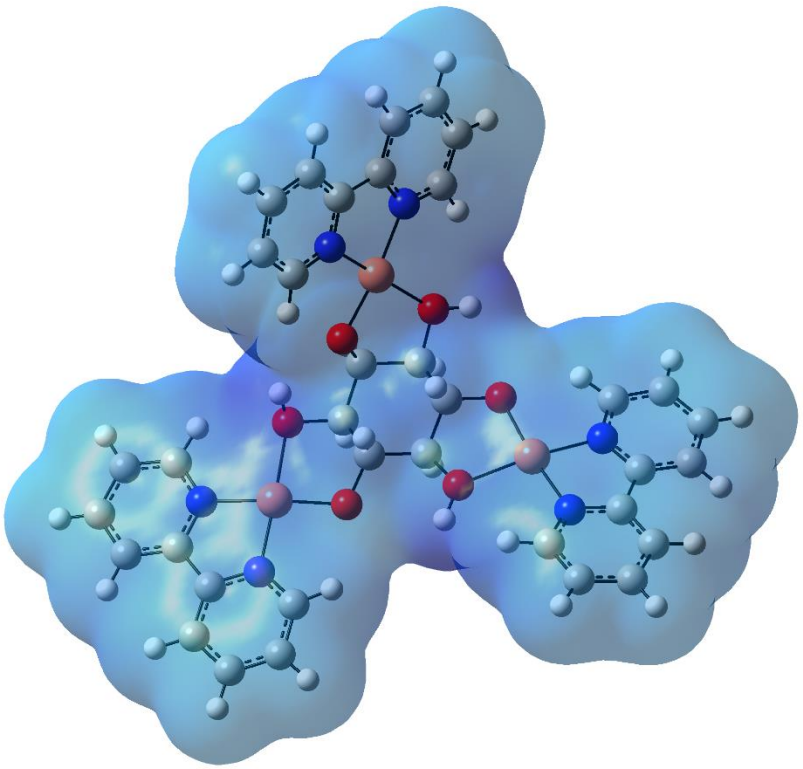

Figure 2.3.7.4 The ESP plots of the metallogelator complex $[Cu_3(H_3ins)(bipy)_3]^{3+}$.

The ESP plots and the energy gap (ΔE_g) have been represented in the **Figure 2.3.7.2** and **Table 2.3.7.1** respectively. The energy gap (ΔE_g), E_{HOMO} and E_{LUMO} values are important for the prediction of global reactivity descriptors, which in details explains the internal charge transfer, stability and reactivity of the molecule[43]. Global reactivity descriptors such as **electronegativity (χ), global hardness (η), global electrophilicity (ω)** and **global softness (σ)** are calculated using the formulas based on Koopmans theorem[44] and are tabulated **(Table 2.3.7.1)**

Table 2.3.7.1 Global reactivity descriptors of complexes in eV calculated by DFT/B3LYP/LANL2DZ basis set

Molecular Properties	Mathematical Description	Values(eV)
E_{HOMO}	Energy of HOMO	**-13.062**
E_{LUMO}	Energy of LUMO	**-9.0257**
Energy gap	$\Delta E_g = E_{LUMO} - E_{HOMO}$	**4.0363**
Ionization potential (IP)	$IP = -E_{HOMO}$	**13.062**
Electron Affinity (EA)	$EA = -E_{LUMO}$	**9.0257**
Electronegativity (χ)	$\chi = -\frac{1}{2}(E_{HOMO} + E_{LUMO})$	**11.04385**
Chemical Potential (μ)	$\mu = \frac{1}{2}(E_{HOMO} + E_{LUMO})$	**-11.04385**
Global Hardness (η)	$\eta = -\frac{1}{2}(E_{HOMO} - E_{LUMO})$	**2.1815**
Softness (S)	$S = 1/2\eta$	**0.2292**
Electrophilicity index (ω)	$\omega = \mu^2/2\eta$	**27.955**

As per the computation, the molecule is an asymmetric top, however, has near C_3 symmetry. It can be seen from the values in **Table 2.3.7.2** and **Figure 2.3.7.2** that the torsional angles around copper(II) are between 160-190 degrees. Thus the coordination geometry around copper is approximately planar. These geometrical features should facilitate π-π stacking between cordinated bipy molecules and also the formation of stacks of the complex ions through coordination or hydrogen bonding with the anions or water molecules. Also, the near planar coordination geometry makes the inositol oxygens available for H-bonding with solvent and interaction with anions.

Table 2.3.7.2 Optimized geometrical parameters involving metal coordination.		
Cu-N Distances (Aº)		
R(24,82)	N24-Cu82	2.0083
R(32,82)	N32-Cu82	1.9934
R(62,83)	N62-Cu83	2.0013
R(68,83)	N68-Cu83	1.9924
R(42,84)	N42-Cu84	1.9926
R(48,84)	N48-Cu84	2.0056
Cu-O Distances (Aº)		
R(8,82)	O8-Cu82	2.0807
R(12,82)	O12-Cu82	1.9118
R(11,83)	O11-Cu83	2.0969
R(7,83)	O7-Cu83	1.9193
R(9,84)	O9-Cu84	2.0551
R(10,84)	O10-Cu84	1.9133
Bond angles		
A(8,82,12)	O8-Cu82-O12	84.4064
A(8,82,24)	O8-Cu82-N24	100.9129
A(12,82,32)	O12-Cu82-N32	94.8474
A(24,82,32)	N24-Cu82-N32	82.3473
A(7,83,11)	O7-Cu83-O12	85.4213
A(7,83,68)	O7-Cu83-N68	95.7818
A(11,83,62)	O11-Cu83-N62	97.3579
A(62,83,68)	N62-Cu83-N68	82.3852
A(9,84,10)	O9-Cu84-O10	83.9133
A(9,84,48)	O9-Cu84-N48	98.6515
A(10,84,42)	O10-Cu84-N42	97.0066
A(42,84,48)	N42-Cu84-N48	82.3591
Torsional angles		
L(8,82,32,24,-1)	O8-Cu82-N32-N24 (-1)	183.2601
L(12,82,24,32,-1)	O12-Cu82-N24-N32 (-1)	177.1946
L(7,83,62,68,-1)	O7-Cu83-N62-N68 (-1)	178.1669
L(11,83,68,62,-1)	O11-Cu83-N68-N62 (-1)	179.743
L(9,84,42,48,-1)	O9-Cu84-N42-N48 (-1)	181.0106
L(10,84,48,42,-1)	O10-Cu84-N48-N42 (-1)	179.3657
L(8,82,32,24,-2)	O8-Cu82-N32-N24 (-2)	163.1729
L(12,82,24,32,-2)	O12-Cu82-N24-N32 (-2)	170.8925
L(7,83,62,68,-2)	O7-Cu83-N62-N68 (-2)	188.0659
L(11,83,68,62,-2)	O7-Cu83-N62-N68 (-2)	186.9341
L(9,84,42,48,-2)	O9-Cu84-N42-N48 (-2)	192.5417
L(10,84,48,42,-2)	O10-Cu84-N48-N42 (-2)	189.0303

2.3.8 Microscopic Properties

Scanning Electron Microscopy of metallogels (SEM)

The gels are formed because of the fibrous assembly. As mentioned before, in the earlier section, the trinuclear complex cation must be forming a one-dimensional supramolecular assembly with help of anions / water / hydroxide. This supramolecular assembly is expected to be resulting in the formation of fibrous network which can entrap water molecules to form the gels. In order to get an insight in the morphology of the metallogels, the scanning electron micrographs of the xerogels were recorded. The SEM images show the formation of compact fibrous structures, wherein each fiber is found to be actually made up of intertwining of thinner fibrils **(Figure 2.3.8.1).** These fibers further appear to organize in the form of various quaternary structures like petals of flowers or the ones diverging away from the center **(Figure 2.3.8.2)**.

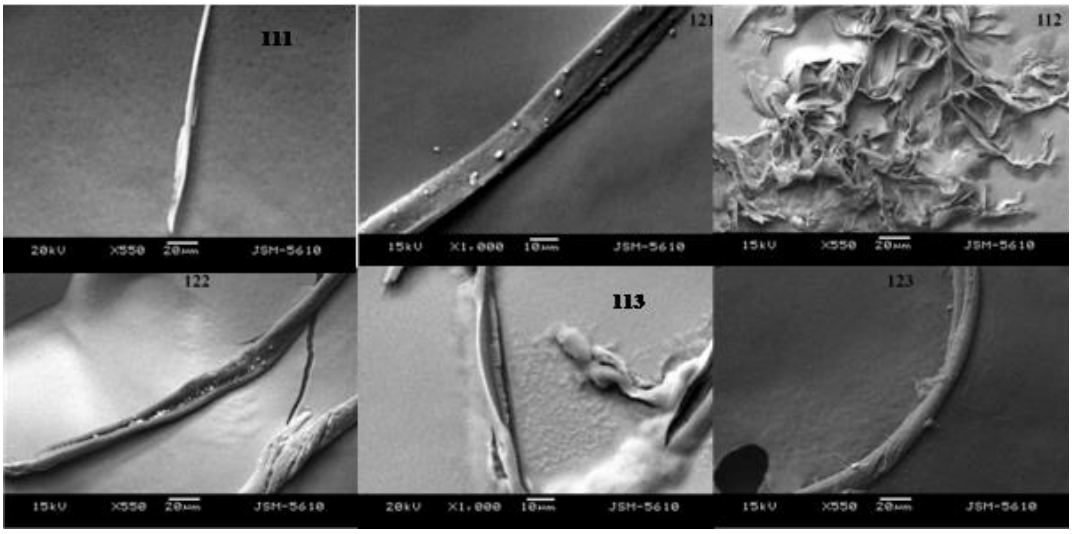

Figure 2.3.8.1 SEM images of xerogels showing the fibrous assemblies.

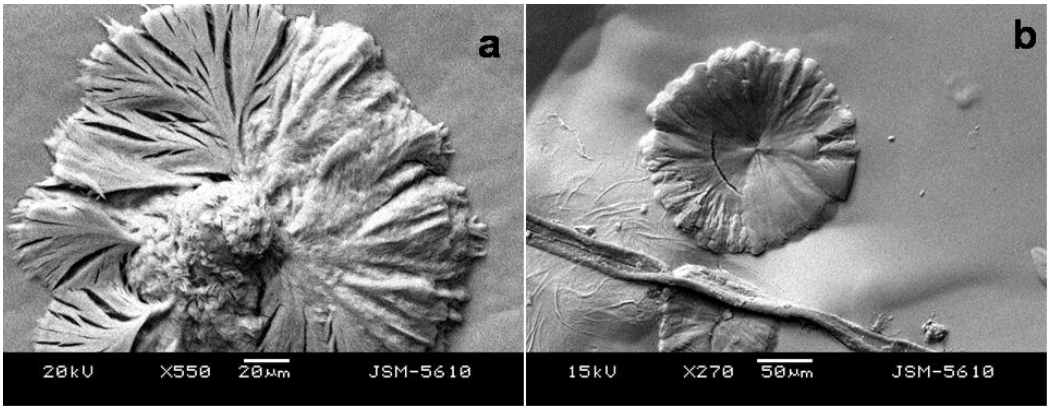

Figure 2.3.8.2 SEM images of xerogels. [a] SEM of image of 111 and [b] SEM image of 121, both showing quaternary structures with flower like pattern.

SEM analysis of the gels further revealed that the thickness of the fibers varied between 8 µm to 20µm **(Figure 2.3.8.3)**. It was further observed that the length of the fibers formed by supramolecular assembly were greater than 400 µm in length indicating strong intermolecular interactions between the complex molecules forming the secondary structure.

The polarized electron micrograph of one of the metallogels-123 was compared to its SEM image which revealed that the thickness of the fibers was similar to what was observed from the SEM analysis **(Figure 2.3.8.3)**.

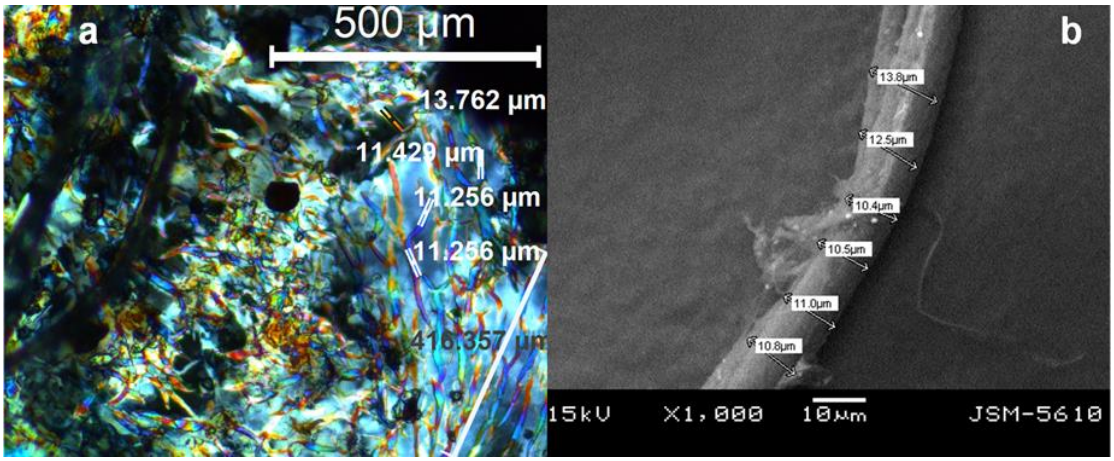

Figure 2.3.8.3 POM image and [b] SEM image of xerogel-**123** showing the fibrous assembly and with their dimensions.

Polarizing Optical Microscopy (POM)

The gel forming complex, being trinuclear has to be dissymmetric having at the most a C_3 symmetry axis. This can induce chirality in the molecule which can further get enhanced by the stacking of molecules and the formation of supramolecular assembly and thus can attribute birefringent property to the gels. In order to examine this possibility and any temperature dependent behaviour, polarizing microscopic studies of the xerogels were carried out.

In order to perform the POM of the xerogels, a drop of the gel was placed on a slide and allowed to dry and convert to a xerogel. As it can be seen in **Figure 2.3.8.4**, the solution of the complex was isotropic and as it gradually changes to a gel, it gets organized and displays birefringent anisotropic behavior when it converts to a xerogel. It was observed that the appearance of the birefringent structures/patterns in the metallogels was temperature independent phenomenon. This behavior, however, was seen to be dependent on the solvent immobilized by the supramolecular assembly and the birefringent patterns can only be observed when the solvent, water in this case, was

lost by the gels and they got converted to xerogels. This change was observed to be reversible with exposure to solvent vapors and its subsequent removal.

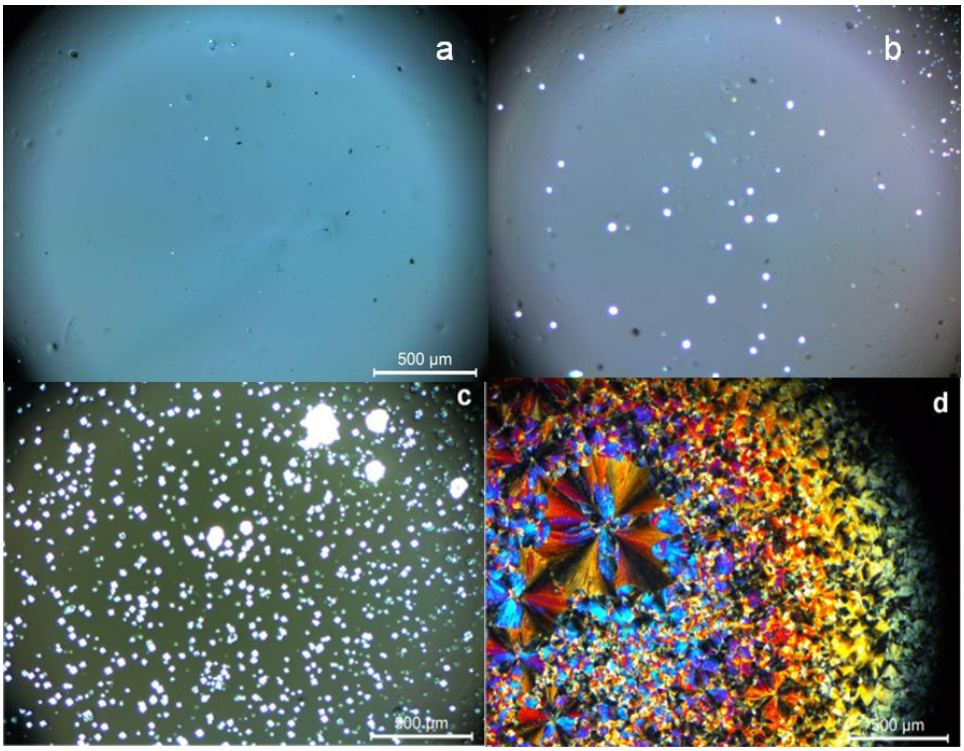

Figure 2.3.8.4 Images [a] to [d] show a gradual change from the isotropic solution to a gel and further to an anisotropic birefringent xerogel.

The POM images captured at various magnifications **(Figure 2.3.8.5 to 2.3.8.10)** show that the assembly was very highly organized and had behaviour like columnar lyotropic[45] or more like smectic thermotropic liquid crystalline phases. As the assembly in gels was captured in the form of xerogel by slow evaporation at low to ambient temperatures, the gels can be called as behaving like lyotropic liquid crystalline phases though the term is not very appropriate.

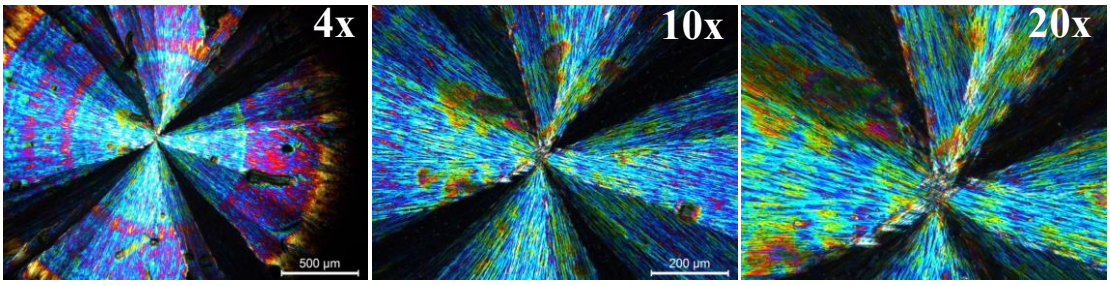

Figure 2.3.8.5 POM images of xerogel **111** at different magnifications **(4x,10x,20x).**

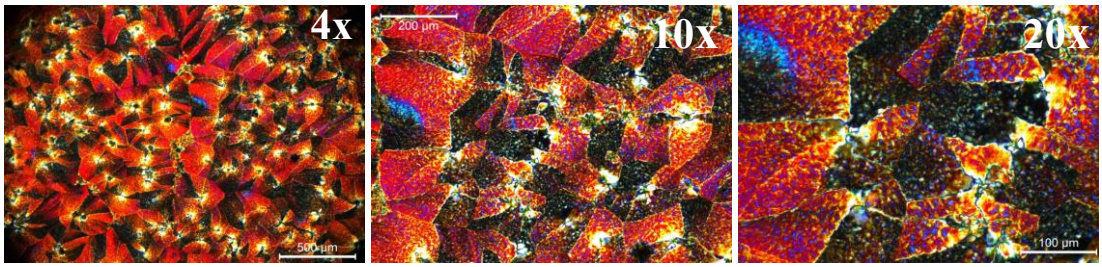

Figure 2.3.8.6 POM images of xerogel **112** at different magnifications **(4x,10x,20x)**.

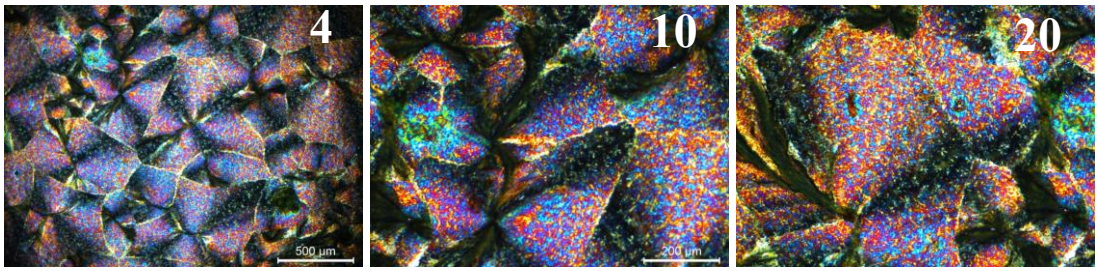

Figure 2.3.8.7 POM images of xerogel **113** at different magnifications **(4x,10x,20x)**.

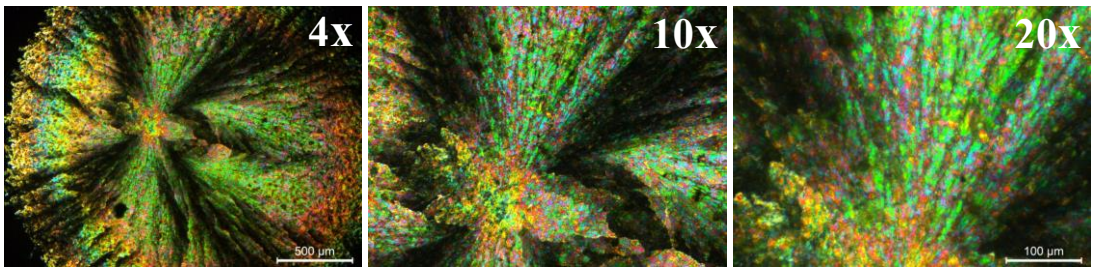

Figure 2.3.8.8 POM images of xerogel **121** at different magnifications **(4x,10x,20x)**.

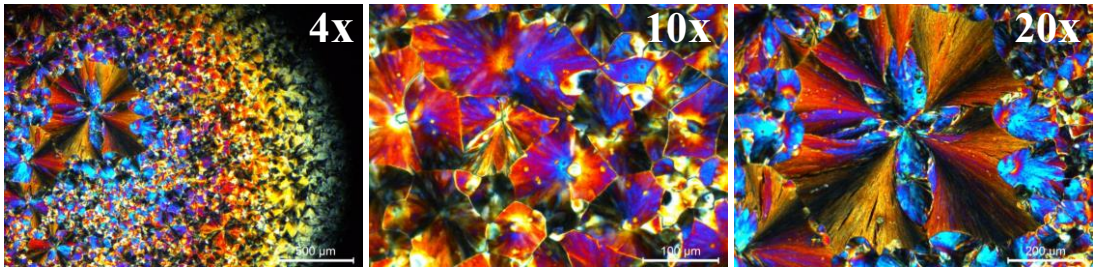

Figure 2.3.8.9 POM images of xerogel **122** at different magnifications **(4x,10x,20x)**.

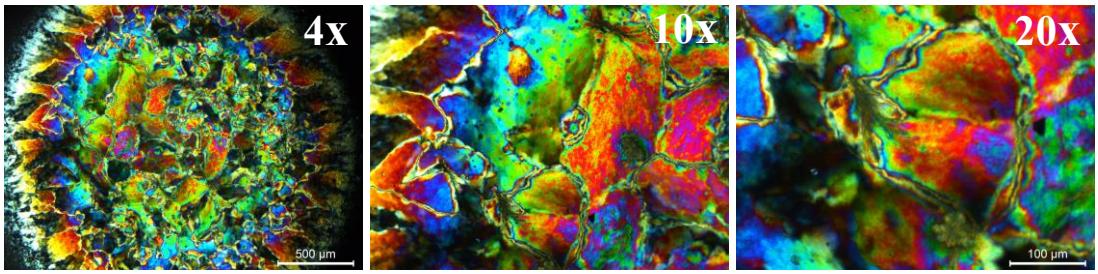

Figure 2.3.8.10 POM images of xerogel **123** at different magnifications **(4x,10x,20x)**.

Birefrigent properties of metallogels

As discussed previously, the complex gelator molecule is dissymmetric and the resulting supramolecular assembly is expected to have birefringent property. The birefringence was explored at different angles of polarizer and analyzer using POM. One of the characteristic properties of birefringent materials is that they respond to the change in the angle between polarizer and the analyzer. The images were captured at different angles of the polarizer and the analyzer **(0, 45, 90, 135).** It can be seen from the images recorded at different angles of polarizer that the assembly is highly birefringent. This type of behavior of these gels, discussed in the present chapter, is very unique **(Figure 2.3.8.11 to Figure 2.3.8.16).**

The reports on the birefringent liquid crystalline gels have been scanty. The only notable report was on thermotropic organo-gel formed by pyridine-2,6-dicarboxamide giving phases between 158-213°C. [15]

The patterns observed in the POM images also depend on the nature of the counter anions. Thus, these counter anions appeared to have significant effect on the supramolecular assembly. As already mentioned earlier, not only that the T_{gel} increased on increasing the alkyl chain length in the carboxylate anion, but the patterns observed in the POM also varied. The gels formed in presence of formate and acetate have unique circular fan shaped organization within which smectic like assembly can be seen.

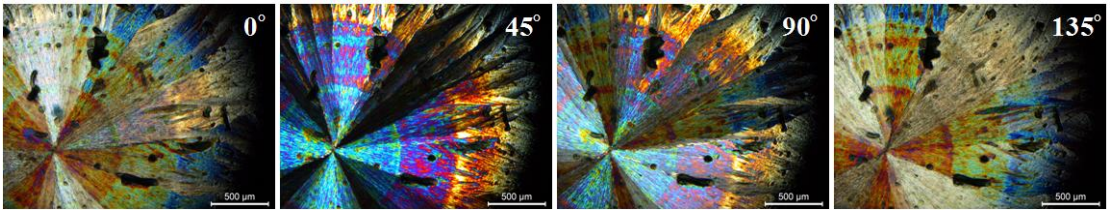

Figure 2.3.8.11 Birefringence and angle dependent POM images of xerogel **111**. **(0, 45, 90, 135)** written after the gel codes on the top right corner in the images represent the angles of polarizer in degrees).

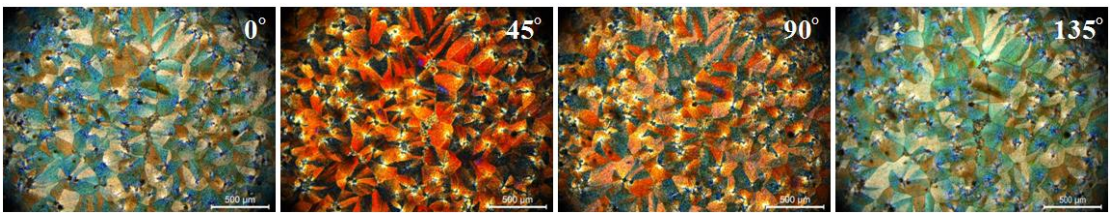

Figure 2.3.8.12 Birefringence and angle dependent POM images of xerogel **112**. **(0, 45, 90, 135)** written after the gel codes on the top right corner in the images represent the angles of polarizer in degrees).

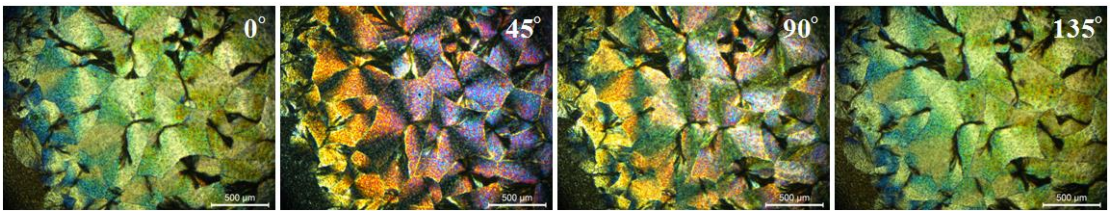

Figure 2.3.8.13 Birefringence and angle dependent POM images of xerogel **113**. **(0, 45, 90, 135)** written after the gel codes on the top right corner in the images represent the angles of polarizer in degrees).

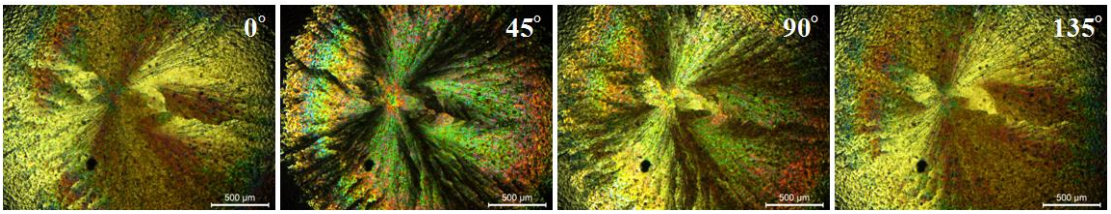

Figure 2.3.8.14 Birefringence and angle dependent POM images of xerogel **121**. **(0, 45, 90, 135)** written after the gel codes on the top right corner in the images represent the angles of polarizer in degrees).

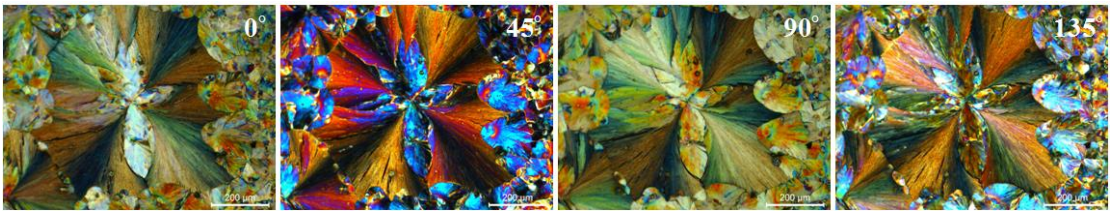

Figure 2.3.8.15 Birefringence and angle dependent POM images of xerogel **122**. **(0, 45, 90, 135)** written after the gel codes on the top right corner in the images represent the angles of polarizer in degrees).

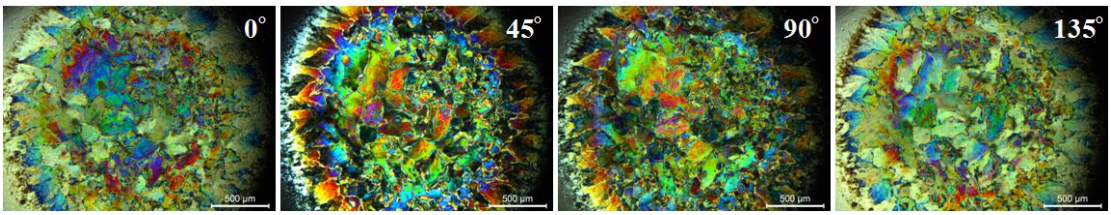

Figure 2.3.8.16 Birefringence and angle dependent POM images of xerogel **123**. **(0, 45, 90, 135)** written after the gel codes on the top right corner in the images represent the angles of polarizer in degrees).

2.3.9 Rheological studies of metallogels

In order to evaluate the mechanical strength and elasticity of the supramolecular gels, their rheological properties were studied. Recently, such studies with organoplatinum(II) containing hydrogels showed that they can be useful not only in characterizing the gels but also in studying their response to certain stimuli like the presence of CO_2.[46,47] The amount of energy stored in the gel system, storage modulus (G'), and the energy dissipated within the system indicated by the loss modulus (G") was measured as a function of frequency **(Fig. 2.3.9.1 to Fig 2.3.9.2).**

A frequency sweep from 0.1 to 50 rad s^{-1} was performed on each gel at a small oscillatory stress of 1.0 Pa at 23 °C. From the rheological studies of all the 3 gels **(121,122,123)** it was observed that the G' and G" curves were linear and parallel, with the storage modulus G' higher than the loss modulus G". The ratio of loss and storage moduli (tan δ = G"/G') was less than 1 and it remained constant at lower frequencies over a wide range, i.e., from 0.1 to 5 rad s^{-1}, which is a characteristic of elastic materials. The tan δ values increased and became >1 with a smooth transition from elastic to viscous behaviour at frequencies higher than 10 rad s^{-1}. This frequency dependence is a characteristic of soft materials[48] and clearly indicates hydrogel-like shear responsive behaviour of the gels discussed in this chapter previously. Further, according to Hvidt's classification,[49,50] these gels can be considered as hard gels as they have G'>1000 Pa.

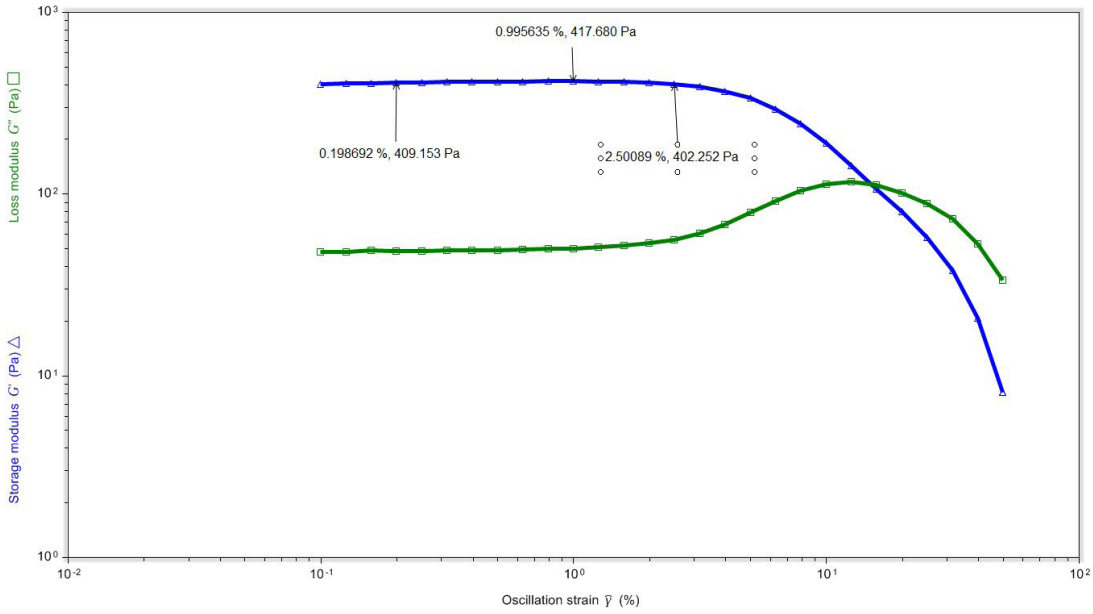

Figure 2.3.9.1 Frequency sweep graph of the gel **121** (Amplitude sweep performed at room temperature @10rad/sec).

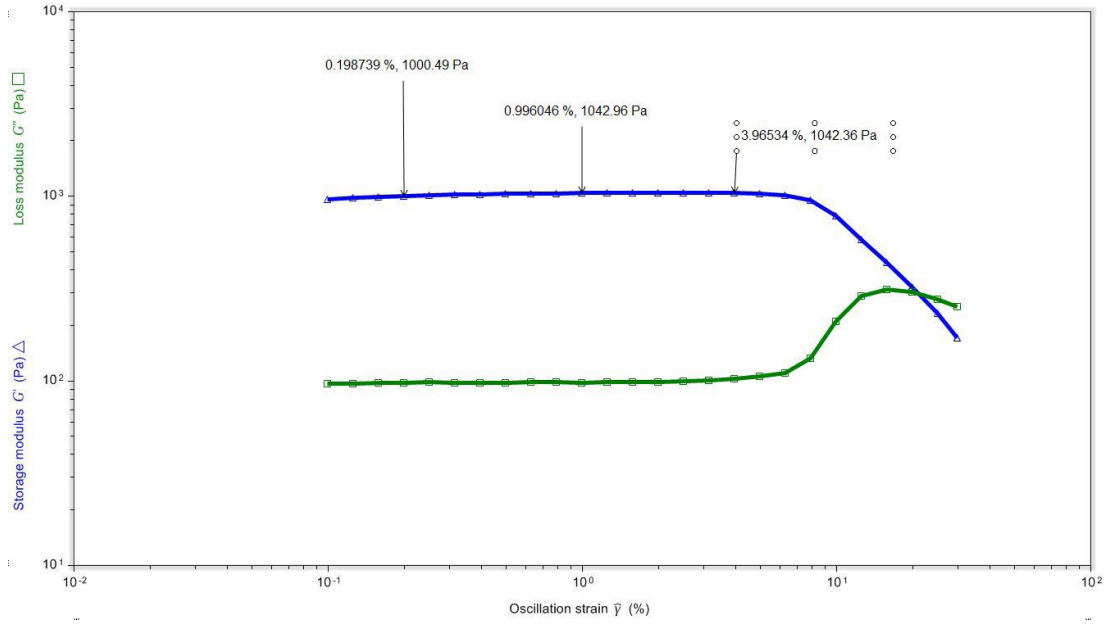

Figure 2.3.9.2. Frequency sweep graph of the gel **122** (Amplitude sweep performed at room temperature @10rad/sec).

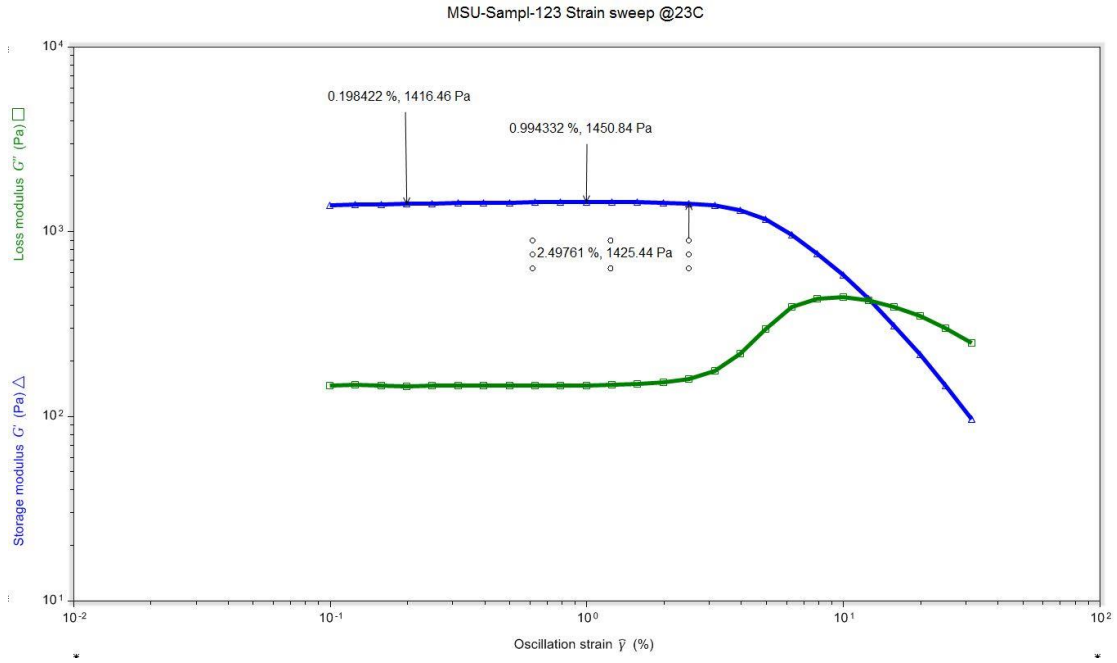

Figure 2.3.9.3. Frequency sweep graph of the gel **123** (Amplitude sweep performed at room temperature @10rad/sec).

2.4 Conclusions

- The trinuclear copper (II) complex of myo-inositol(ins) and 2,2'-bipyridine(bipy), **$[Cu_3(H_3ins)(bipy)_3]X_3$**, in which X was varied as $HCOO^-$, CH_3COO^- and $CH_3CH_2COO^-$ were synthesized.

- The complex organized in the form of a supramolecular assembly in presence of caustic alkali at pH 12, which resulted in metallogel formation.

- The metallogels have been characterized by thermal analysis and spectroscopic methods. The SEM analysis indicated the presence of fibrous supramolecular assembly.

- The metallogels were found to be highly birefringent and they organized into quaternary structures which displayed unique patterns in the microscopic studies under polarized light. The birefringence in the metallogels resulted because of the presence of dissymmetry in the gel-forming complex cation.

- The formation of gels and their properties including T_{gel} were found to dependent greatly on the presence of various carboxylates and the alkali used.

- The anions were also found to significantly affect the quaternary assemblies which could be seen in the microscopic images under polarized light.

References

1. Abdallah, B. D. J. & Weiss, R. G. Organogels and Low Molecular Mass Organic Gelators. *Adv. Mater.* **12**, 1237–1247 (2000).
2. Terech, P. & Weiss, R. G. Low Molecular Mass Gelators of Organic Liquids and the Properties of Their Gels. *Chem. Rev.* **2665**, 3133−3159 (1997).
3. *Molecular Gels: Materials With Self- Assembled Fibrillar Networks, (Eds. R. G. Weiss and P. Terech)*. (Springer, Dordrecht, 2006).
4. Dastidar, P. Supramolecular gelling agents : can they be designed ? *Chem. Soc. Rev.* **37**, 2699–2715 (2008).
5. Esch, J. H. Van & Feringa, B. L. New Functional Materials Based on Self-Assembling Organogels : From Serendipity towards Design. *Angew. Chem. Int. Ed.* **39**, 2263–2266 (2000).
6. Xing, B., Choi, M. F. & Xu, B. A stable metal coordination polymer gel based on a calix[4]arene and its "uptake" of non-ionic organic molecules from the aqueous phase. *Chem. Commun.* 362–363 (2002).
7. Estroff, L. A. & Hamilton, A. D. Water Gelation by Small Organic Molecules Lara. *Chem. Rev.* **104**, 1201–1218 (2004).
8. Babu, S. S., Praveen, V. K. & Ajayaghosh, A. Functional π-gelators and their applications. *Chem. Rev.* **114**, 1973–2129 (2014).
9. Fenniri, H., Mathivanan, P., Vidale, K. L., Sherman, D. M., Hallenga, K., Wood, K. V. & Stowell, J. G. Helical rosette nanotubes: Design, self-assembly, and characterization. *J. Am. Chem. Soc.* **123**, 3854–3855 (2001).
10. Israelachvili, J. N. *Intermolecular and Surface Forces*. (Academic Press, New York, 3rd edn, 1991).
11. Ajayaghosh, A. & George, S. J. First phenylenevinylene based organogels: Self-assembled nanostructures via cooperative hydrogen bonding and π-stacking. *J. Am. Chem. Soc.* **123**, 5148–5149 (2001).
12. Hui, J. K. H. & MacLachlan, M. J. Metal-containing nanofibers via coordination chemistry. *Coord. Chem. Rev.* **254**, 2363–2390 (2010).
13. Tatikonda, R., Bertula, K., Nonappa, Hietala, S., Rissanen, K. & Haukka, M. Bipyridine based metallogels: an unprecedented difference in photochemical and chemical reduction in the in situ nanoparticle formation. *Dalt. Trans.* **46**, 2793–2802 (2017).
14. Denzer, B. R., Kulchar, R. J., Huang, R. B. & Patterson, J. Advanced methods for the characterization of supramolecular hydrogels. *Gels* **7**, 1–29 (2021).
15. Shen, Y., Li, C., Chang, K., Chin, S., Lin, H., Liu, Y., Hung, C., Hsu, H. & Sun, S. Synthesis, Optical, and Mesomorphic Properties of Self-Assembled Organogels Featuring Phenylethynyl Framework with Elaborated Long-Chain Pyridine-2,6-Dicarboxamides. *Langmuir* **25**, 8714–8722 (2009).
16. Rodr, F., Escuder, B., Hamley, I. W. & Miravet, J. F. Structural and morphological studies of the dipeptide based L -Pro- L -Val organocatalytic gels and their rheological behaviour. *Soft Matter* **8**, 8865–8872 (2012).
17. Magill, J. H. Spherulites: A personal perspective. *J. Mater. Sci.* **36**, 3143–3164

(2001).

18. Bassett, D. C. Polymer spherulites: A modern assessment. *J. Macromol. Sci. Part B Phys.* **42**, 227–256 (2003).
19. Moriyama, M., Mizoshita, N., Yokota, T., Kishimoto, K. & Kato, T. Photoresponsive Anisotropic Soft Solids : *Adv. Mater* **15**, 1335–1338 (2003).
20. Moriyama, M., Mizoshita, N. & Kato, T. Reversible On – Off Photo- switching of Hydrogen Bonding for Self-Assembled Fibers Comprising Physical Gels. *Bull. Chem. Soc. Jpn.* **79**, 962–964 (2006).
21. Ruan, H., Chen, G., Zhao, X., Wang, Y., Liao, Y., Peng, H., Feng, C. L., Xie, X. & Smalyukh, I. I. Chirality-Enabled Liquid Crystalline Physical Gels with High Modulus but Low Driving Voltage. *ACS Appl. Mater. Interfaces* **10**, 43184–43191 (2018).
22. Oriyama, M. M., Izoshita, N. M. & Ato, T. K. Photopatterning of Discotic Liquid-Crystalline Gels. *Polym. J.* **36**, 661–664 (2004).
23. Zhao, Y. & Tong, X. Light-induced reorganization in self-assembled liquid crystal gels: Electrically switchable diffraction gratings. *Adv. Mater.* **15**, 1431–1435 (2003).
24. Bairi, P., Roy, B. & Nandi, A. K. pH and anion sensitive silver (I) coordinated melamine hydrogel with dye absorbing properties : metastability at low melamine concentration. *J. Mater. Chem.* **21**, 11747–11749 (2011).
25. Dey, S., Datta, D., Chakraborty, K., Nandi, S., Anoop, A. & Pathak, T. A coordination-assisted general approach to nickel- based nano metallogels. *RSC Adv.* **3**, 9163–9166 (2013).
26. Taylor, M. J., Tomlins, P. & Sahota, T. S. Thermoresponsive gels. *Gels* **3**, 1–31 (2017).
27. Yan Chen, Hu, C., Fang, Z. & Mao, J. K2Pb(H2C3N3O3)4(H2O)4: a potential UV nonlinear optical material with large birefringence. *Inorg. Chem. Front.* **8**, 3547–3555 (2021).
28. Puranik, A. A. & Kulkarni, N. D. Supramolecular Birefringent Metallohydrogels formed by Trinuclear Copper (II) complexes containing myo-inositol. *New J. Chem.* **3**, 1–23.
29. Vosko, S. H., Wilk, L. & Nusair, M. Accurate spin-dependent electron liquid correlation energies for local spin density calculations: a critical analysis. *Can. J. Phys.* **58**, 1200–1211 (1980).
30. Stephens, P. J., Devlin, F. J., Chabalowski, C. F. & Frisch, M. J. Ab Initio calculation of vibrational absorption and circular dichroism spectra using density functional force fields. *J. Phys. Chem.* **98**, 11623–11627 (1994).
31. Becke, A. D. Density-functional thermochemistry. III. The role of exact exchange. *J. Chem. Phys.* **98**, 5648–5652 (1993).
32. Lee, C., Yang, W. & Parr, R. G. Development of the Colle-Salvetti correlation-energy formula into a functional of the electron density. *Physcial Rev. B* **37**, 785–789 (1988).
33. McLean, A. D. & Chandler, G. S. Contracted Gaussian basis sets for molecular calculations. I. Second row atoms, Z=11-18. *J. Chem. Phys.* **72**, 5639–5648

(1980).
34. Krishnan, R., Binkley, J. S., Seeger, R. & Pople, J. A. Self-consistent molecular orbital methods. XX. A basis set for correlated wave functions. *J. Chem. Phys.* **72**, 650–654 (1980).
35. Frisch, M. J., Trucks, G. W., Schlegel, H. B., Scuseria, G. E., Robb, M. A., Cheeseman, J. R., Scalmani, G., Barone, V., Petersson, G. A., Nakatsuji, H., Li, X., Caricato, M., Marenich, A. V, Bloino, J., Janesko, B. G., Gomperts, R., Mennucci, B., Hratchian, H. P., *et al.* Gaussian 16, Revision A.03. *Gaussian, Inc., Wallingford CT* (2016).
36. Dennington, R., Keith, T. A. & Millam, J. M. GaussView 6. (2016).
37. Hirao, H. & Morokuma, K. Insights into the (superoxo)Fe(III)Fe(III) intermediate and reaction mechanism of myo-inositol oxygenase: DFT and ONIOM(DFT:MM) study. *J. Am. Chem. Soc.* **131**, 17206–17214 (2009).
38. Spiers, I. D., Barker, C. J., Chung, S. K., Chang, Y. T., Freeman, S., Gardiner, J. M., Hirst, P. H., Lambert, P. A., Michell, R. H., Poyner, D. R., Schwalbe, C. H., Smith, A. W. & Solomons, K. R. H. Synthesis and iron binding studies of myo-inositol 1,2,3-trisphosphate and (±)-myo-inositol 1,2-bisphosphate, and iron binding studies of all myo-inositol tetrakisphosphates. *Carbohydr. Res.* **282**, 81–99 (1996).
39. Blank, G. Magnesium Ion Binding to myo-Inositol: The Crystal Structure of myo-Inositol-Magnesium Chloride-Hydrate (1 : 1 : 4). *Acta Cryst* **B29**, 1677–1683 (1973).
40. Persson, H., Turk, M., Nyman, M. & Sandberg, A. S. Binding of Cu2+, Zn2+, and Cd2+ to inositol tri-, tetra-, penta-, and hexaphosphates. *J. Agric. Food Chem* **46**, 3194–3200 (1998).
41. Hu, H., Xue, J., Wen, X., Li, W., Zhang, C., Yang, L., Xu, Y., Zhao, G., Bu, X., Liu, K., Chen, J. & Wu, J. Sugar-metal ion interactions: The complicated coordination structures of cesium ion with d-ribose and myo-inositol. *Inorg. Chem.* **52**, 13132–13145 (2013).
42. Fukui, K. Role of Frontier Orbitals in Chemical Reactions. *Science (80-.).* **218**, 747–754 (1982).
43. Jawaria, R., Hussain, M., Khalid, M., Khan, M. U., Tahir, M. N., Naseer, M. M., Braga, A. A. C. & Shafiq, Z. Synthesis, crystal structure analysis, spectral characterization and nonlinear optical exploration of potent thiosemicarbazones based compounds: A DFT refine experimental study. *Inorganica Chim. Acta* **486**, 162–171 (2019).
44. Koopmans, T. Über die Zuordnung von Wellenfunktionen und Eigenwerten zu den Einzelnen Elektronen Eines Atoms. *Physica* **1**, 104–113 (1934).
45. *Handbook of Liquid Crystals*. (Wiley-VCH, Weinheim, 1998).
46. Zheng, W., Chen, L. J., Yang, G., Sun, B., Wang, X., Jiang, B., Yin, G. Q., Zhang, L., Li, X., Liu, M., Chen, G. & Yang, H. B. Construction of Smart Supramolecular Polymeric Hydrogels Cross-linked by Discrete Organoplatinum(II) Metallacycles via Post-Assembly Polymerization. *J. Am. Chem. Soc.* **138**, 4927–4937 (2016).

47. Zheng, W., Yang, G., Shao, N., Chen, L. J., Ou, B., Jiang, S. T., Chen, G. & Yang, H. B. CO2 stimuli-responsive, injectable block copolymer hydrogels cross-linked by discrete organoplatinum(II) metallacycles via stepwise post-assembly polymerization. *J. Am. Chem. Soc.* **139**, 13811–13820 (2017).
48. Stokes, J. R. & Frith, W. J. Rheology of gelling and yielding soft matter systems. *Soft Matter* **4**, 1133–1140 (2008).
49. Almgren, M., Brown, W. & Hvidt, S. Self-aggregation and phase behavior of poly(ethylene oxide)-poly(propylene oxide)-poly(ethylene oxide) block copolymers in aqueous solution. *Colloid Polym. Sci.* **273**, 2–15 (1995).
50. Hvidt, S., Jørgensen, E. B., Brown, W. & Schulen, K. Micellization and gelation of aqueous solutions of a triblock copolymer studied by rheological techniques and scanning calorimetry. *J. Phys. Chem.* **98**, 12320–12328 (1994).

•